Effects of surface thermodynamics on hydrogen isotope exchange kinetics in palladium: Particle and flow models

ARTICLE *in* CHEMICAL ENGINEERING SCIENCE · JANUARY 2015

Impact Factor: 2.34 · DOI: 10.1016/j.ces.2014.09.001

3 AUTHORS, INCLUDING:

Maher Salloum

Sandia National Laboratories

42 PUBLICATIONS **389** CITATIONS

SEE PROFILE

Scott C James

Baylor University

128 PUBLICATIONS **730** CITATIONS

SEE PROFILE

Chemical Engineering Science 122 (2015) 474–490

Contents lists available at ScienceDirect

Chemical Engineering Science

journal homepage: www.elsevier.com/locate/ces

Effects of surface thermodynamics on hydrogen isotope exchange kinetics in palladium: Particle and flow models

Maher Salloum *, Scott C. James, David B. Robinson

Sandia National Laboratories, 7011 East Ave., MS 9158, Livermore, CA 94550, USA

HIGHLIGHTS

- A detailed surface reaction is incorporated into models of hydrogen isotope exchange in palladium.
- Surface hydride stability causes a large activation barrier and strong temperature dependence.
- The transition between solid-phase diffusion- and surface-limited reactions is delineated.
- The model identifies conditions for optimal performance of isotope exchange columns.

GRAPHICAL ABSTRACT

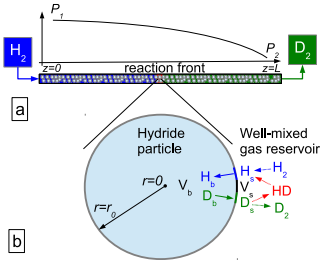

ARTICLE INFO

Article history:
Received 12 March 2014
Received in revised form
15 July 2014
Accepted 4 September 2014
Available online 16 September 2014

Keywords:
Adsorption
Hydride
Activation Barrier
Chromatography
Pressure Drop
Isotope Exchange

ABSTRACT

Palladium is an important material for separation of hydrogen from other gases, separation of hydrogen isotopes, and for hydrogen storage. Its main advantages are its high selectivity and rapid, highly reversible uptake and release of hydrogen at near-ambient temperatures and pressures. Toward a more comprehensive understanding of its behavior, we present particle and continuum multiphysics mathematical models of the coupled reactive transport of hydrogen isotopes in the context of a single palladium sphere, and of flow in a packed palladium hydride bed. The models consider rates of chemical reactions and mass transport within a hydride bed, and incorporate a multistep reaction mechanism involving the metal bulk, metal surface, and gas phases. A unique feature in this formulation is that the chemical reaction model accounts for all absorption, adsorption, and diffusion activation energies. In particular, the adsorption energy is believed to depend strongly on the composition and atom-scale structure of the surface. We perform a parametric study to evaluate the effects of temperature, surface adsorption energy, and hydride particle radius on the isotope exchange kinetics. The models are useful in designing optimal hydride beds operating at various temperatures, with varied hydride particle size, and surface conditions.

1. Introduction

Palladium and its alloys can absorb and release hydrogen under mild conditions with relatively little structural change. While too expensive for large-scale hydrogen storage, the metal has proven useful for separation. No other gases can easily enter and leave palladium, so it can serve as a membrane for highly selective separation of hydrogen from other gases in industrial processes (Ward and Dao, 1999). In a mixture of hydrogen isotopes, lighter isotopes have a significantly stronger preference for absorption, so this metal has proven valuable for isotope separation (Heung et al., 2011).

The performance of palladium in these applications is strongly sensitive to conditions at the surface. Dissociative adsorption of hydrogen is an intermediate step to its absorption, and the surface is also an intermediate during the reverse process. In gas separation applications, trace amounts of other reactive gases such as carbon

* Corresponding author.
E-mail address: mnsallo@sandia.gov (M. Salloum).

http://dx.doi.org/10.1016/j.ces.2014.09.001
0009-2509/

monoxide or hydrogen sulfide can block hydrogen adsorption sites (Outka and Foltz, 1991), and significantly reduce rates of hydrogen transport through a membrane. This can be alleviated by alloying, and operating at elevated temperatures, among other strategies to facilitate desorption of blocking species (Paglieri and Way, 2002; Yun and Oyama, 2011). Transport rates are slow at low temperatures, in part because the surface hydride is quite stable, and must overcome a high activation barrier to absorb into the bulk metal or desorb as a diatomic gas molecule. Surface modifications have been proposed with the goal of destabilizing the surface hydride (Greeley and Mavrikakis, 2005).

As new strategies emerge to address these performance issues, it is helpful to have a theoretical model for a separation process that can evaluate the mechanisms behind each strategy, and account for the various phenomena that occur simultaneously, in order to determine which of them have the most important effects. Such a model should straightforwardly map to the results of experiments that can rapidly and clearly test the same hypotheses.

Isotope exchange is a valuable experimental technique that can be connected to an established modeling approach (Foltz and Melius, 1987). In this technique, one isotope, *e.g.* deuterium (D), is stored in the solid powdered-metal phase. Another isotope, *e.g.*, protium (H) flows through the Pd powder such that deuterium is extracted from the powder and replaced with protium. The key advantage of this experiment is that it facilitates study of hydrogen-isotope reaction kinetics and transport rates independently of the rates of Pd lattice expansion and contraction that occur when the total amount of hydrogen isotopes stored in the Pd varies significantly. The focus of this paper will be limited to the isotope exchange reaction involving Pd hydride in the concentrated (β) phase; we emphasize that it does not directly apply to cases involving the dilute (α) hydride phase or mixed-phase systems.

Isotope exchange has been the subject of several experimental and theoretical studies (Foltz and Melius, 1987; Outka and Foltz, 1991; Fukada et al., 1995; Charton et al., 1999; Bakaev, 2009; Larson et al., 2011; James et al., 2012). Among the earliest reported studies is that of Foltz and Melius (1987) who developed a simple mathematical model of the two-way isotope exchange of protium and deuterium in Pd. They also performed experiments by injecting one isotope as a gas through a cylindrical powder bed, and measured the gas composition at the bed outlet. Using appropriate reaction rates, good agreement was found between the measured and simulated gas composition at the bed outlet. Outka and Foltz (1991) later extended this to account for blocking of adsorption sites by reactive gases. A similar model was fit to experimental data to derive an isotope separation factor that varied with temperature (Fukada et al., 1995). A more recent model improved the model of Foltz and Melius by considering the effects of temperature and pressure on the stoichiometry and gas compositions (Charton et al., 1999). These models do not explicitly connect the thermodynamics and kinetics of the metal surface. They are based on the assumption that the isotope exchange is limited by either the kinetics of the surface reaction or the diffusion of hydride in the solid. The former case is dominant for small powder particles and/or high temperatures, while the latter case is dominant for large particles and low temperatures. It is of industrial significance to have control over these factors. For example, decreasing the surface adsorption energy may result in a faster isotope exchange, hence a faster process. Previous studies of separation membranes (Ward and Dao, 1999) and catalysis of reactions involving hydrogen (Greeley and Mavrikakis, 2005) have examined the importance of surface thermodynamics on these applications. The studies of Larson et al. (2011) advanced the thermodynamic treatment of the Foltz and Melius approach. James et al. (2012) also developed a detailed model of solid-phase diffusion of hydride and deuteride.

We seek a more detailed understanding of how surface kinetics affect exchange rates, and how surface thermodynamics affect surface kinetics. In particular, the surface hydride of palladium is more thermodynamically stable than the bulk hydride. This leads to a high occupancy of surface sites, and an activation barrier to surface-to-bulk transport. Chemical modification of the surface, such as creation of a near-surface alloy, is expected to destabilize the surface hydride, making it easier for surface hydrides to overcome the activation barrier to the bulk state, and increase the population of surface vacancies (Greeley and Mavrikakis, 2005). Varying the surface energy in a model aids understanding of its impact on predicted exchange rates.

The focus of this paper is to develop a detailed surface chemical kinetics model and to couple it to the most recent models of gas flow (Larson et al., 2011) and hydride diffusion in the solid phase (James et al., 2012), to create a more complete mathematical model of an isotope exchange reactor, thereby allowing comparison of flow rates, rates of transport through the surface, and bulk diffusion rates all within a single, unified model. However, the transport phenomena involved in such a detailed model spread over different time and length scales. Accounting for these phenomena simultaneously requires the discretization of both the gas-flow domain and the solid-particle domain, making the computational cost unreasonably high. Instead, two sub-models are developed. In the first sub-model, the particle-diffusion model of James et al. (2012) is coupled with the detailed surface-kinetics model. The results of this sub-model enable us to assess whether the surface kinetics or the bulk particle diffusion is rate limiting depending on the particle size, the temperature, and the surface adsorption energy. When this sub-model informs us that the particle diffusion is not rate limiting and can be neglected, the second sub-model can be used. In this model, the one-dimensional reactive gas flow model of Larson et al. (2011) is coupled with the detailed surface kinetics model. It is a model of an isotope exchange experiment in a cylindrical palladium hydride bed that accounts for the dependence of overall reaction kinetics on the thermodynamics of surface states. These two sub-models are sketched in Fig. 1.

2. Chemical reactions

The exchange of hydrogen and deuterium between the gas phase and the solid phase takes place in four successive steps. First, the gas is transported to the near-surface by mass convection through the boundary layer adjacent to the surface of the particles.

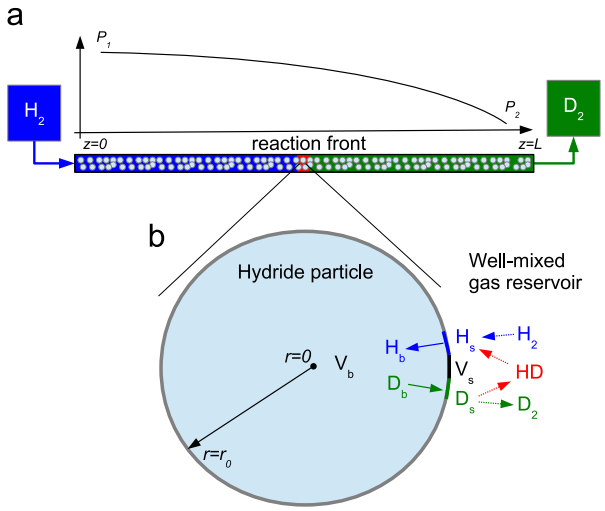

Fig. 1. Schematics of the two sub-models of hydrogen isotope exchange developed in this paper. (a) The one-dimensional reactive gas flow model coupled with the detailed surface kinetics model. The reactor tube is filled with palladium powder and connected to two tanks at pressures P_1 and P_2. (b) A magnified view around one palladium spherical particle of radius r_0 showing the particle-diffusion model coupled with the detailed surface-kinetics model. The species V is a vacancy. The subscripts 'b' and 's' denote bulk and surface species, respectively.

We will focus on cases where this process is anticipated to be fast compared to surface reaction and solid transport. Second, the gas molecules dissociate and fill the solid-particle surface sites. Third, the hydrogen isotopes at surface sites are transported to the solid bulk near the surface. Fourth, they diffuse deeper into the bulk. The reverse processes take place simultaneously. Particles are assumed to be nonporous in this work. Larson et al. (2011) provide a description of the surface reactions of each step adopted here. Adsorption of H_2, HD, and D_2 gases onto surface sites (vacant V_s, H-occupied H_s, and D-occupied D_s) are:

$$H_2 + 2V_s \underset{k_{des,H}}{\overset{k_{ads,H}}{\rightleftharpoons}} 2H_s, \tag{R1}$$

$$HD + 2V_s \underset{k_{des,HD}}{\overset{k_{ads,HD}}{\rightleftharpoons}} H_s + D_s, \tag{R2}$$

$$D_2 + 2V_s \underset{k_{des,D}}{\overset{k_{ads,D}}{\rightleftharpoons}} 2D_s, \tag{R3}$$

where the ks are the forward and reverse reaction rate constants, the subscripts of which provide a name for each reaction. Transport from surface sites to bulk sites (vacant V_b, H-occupied H_b, and D-occupied D_b) are:

$$H_s + V_b \underset{k_{bs,H}}{\overset{k_{sb,H}}{\rightleftharpoons}} H_b + V_s, \tag{R4}$$

$$D_s + V_b \underset{k_{bs,D}}{\overset{k_{sb,D}}{\rightleftharpoons}} D_b + V_s. \tag{R5}$$

Reactions of gas phase molecules with the solid involving no net change in surface concentrations (Larson et al., 2011) are governed by the following equations:

$$H_2 + 2V_b \rightleftharpoons 2H_b, \tag{R6}$$

$$H_2 + D_2 \rightleftharpoons 2HD, \tag{R7}$$

$$D_2 + 2V_b \rightleftharpoons 2D_b. \tag{R8}$$

Reactions (R6)–(R8) do not imply a separate reaction mechanism from reactions (R1)–(R5), but simply express net reactions that can be related to experimental data. Such data on reactions (R6)–(R8) will help eliminate unknown parameters in the model. The transport in the bulk is assumed to follow the model described by James et al. (2012), which includes an activation barrier for the diffusion constant. Rate laws for the chemical reactions are coupled to gas-phase transport models, and relate the thermodynamics of each state to kinetics. We apply a simple model where each reaction is characterized by an Arrhenius rate constant, with an activation energy and an attempt frequency. Reaction rates are assumed to be proportional to concentrations of each reactant. Many complications to this model are potentially significant, such as distributions of energy states on the surface and in the bulk, and neighbor interactions on the surface and in the bulk. For this work, these are neglected to focus on evaluating the utility and limitations of this less complicated model. One of our goals is to identify activation energies based on experimentally measured enthalpies. For the attempt frequencies, measured prefactors for similar chemical reactions or transport processes are used because they include the entropic contribution to the activation free energy. Where these are not available, we rely on vibrational frequencies in bound states, or gas-phase velocities, which can be measured or predicted separately. These assumptions do not incorporate the entropic contribution. The suitability of these assumptions will be evaluated in the future through comparison to experimental data.

Ward and Dao present a useful description of the relationships between activation energies (Ward and Dao, 1999). A slightly rearranged version, defining three activation energies, E_{ads}, E_{abs}, and E_{diff} (kJ per mol of H or D atomic species), is depicted in Fig. 2.

2.1. Rate of production of surface species

The model requires the molar production rate of each species per unit area of metal hydride, s_i (mol cm^{-2} s^{-1}), where the subscripts i are any of the reaction species. These values will be related to molar production rates per unit volume in different ways for each of the particle model and the bed model (see Section 3). The rates s_i of formation of diatomic gas species can be constructed from rate laws for the reactions as follows:

$$s_{H_2} = \omega_{des,H} \exp\left(\frac{2E_{ads,H}}{RT}\right)\frac{H_s^2}{\Gamma_s} - \nu_{H_2}\left(\frac{V_s}{\Gamma_s}\right)^2 [H_2], \tag{1}$$

$$s_{HD} = \omega_{des,HD} \exp\left(\frac{E_{ads,HD}}{RT}\right)\frac{H_s D_s}{\Gamma_s} - \nu_{HD}\left(\frac{V_s}{\Gamma_s}\right)^2 [HD], \tag{2}$$

$$s_{D_2} = \omega_{des,D} \exp\left(\frac{2E_{ads,D}}{RT}\right)\frac{D_s^2}{\Gamma_s} - \nu_{D_2}\left(\frac{V_s}{\Gamma_s}\right)^2 [D_2], \tag{3}$$

where $R = 8.314$ J mol^{-1} K^{-1} is the universal gas constant, T is the temperature (K), and Γ_s is the total surface concentration of filled and vacant sites (mol cm^{-2}). The concentration of the surface vacancies is recovered by:

$$V_s = \Gamma_s - H_s - D_s. \tag{4}$$

The first term on the right-hand sides of Eqs. (1)–(3) is the rate of recombinative desorption. H_s, D_s, and V_s are the area concentration of surface hydrides, deuterides, and vacant sites (mol cm^{-2}). Note that $E_{ads,H}$ and $E_{ads,D}$ correspond to monoatomic species whereas $E_{ads,HD}$ corresponds to a diatomic molecule. Factors such as H_s^2/Γ_s are concentrations of adjacent reactant pairs on the surface. These are multiplied by a desorption attempt frequency ω_{des} (Hz) and a probability that each attempt overcomes the energetic barrier to desorption of each species, E_{ads}. These can be measured (Ward and Dao, 1999) or calculated independently. Our formulation differs from that of Ward and Dao (1999) who lump the ω and Γ terms into rate constants, and/or lump the Γ terms into the concentrations to create unitless measures of surface or bulk occupancy.

The second term in each of (1)–(3) is the rate of dissociative adsorption. Following Ward and Dao (1999), we assume that adsorption is activationless, and that a gas molecule that collides

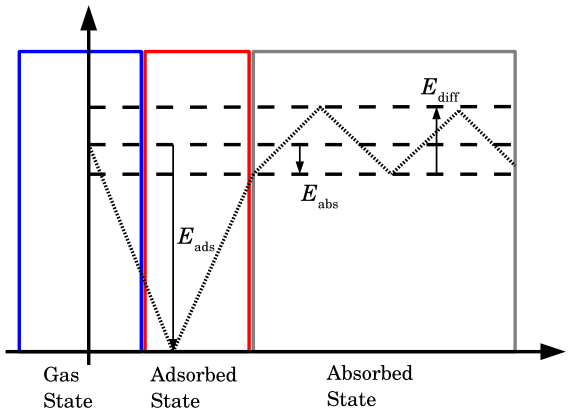

Fig. 2. A schematic representing the free energies of each species. These may exist in the gas phase as a diatomic molecule (on the left of the figure), which can dissociatively adsorb from the gas into a deep well (with no activation energy) as a surface hydride with reaction enthalpy $2E_{ads}$, or go from the gas phase into the bulk with net reaction enthalpy $2E_{abs}$, and from there overcome a diffusional activation barrier E_{diff} to enter a deeper state, or the reverse of each of these. The activation barrier from the surface to the gas phase is $-2E_{ads}$, and from the surface to bulk is $E_{diff} + E_{abs} - E_{ads}$. The figure is adapted from Ward and Dao (1999).

with a pair of vacancies on the surface will react. The products of the mean thermal gas velocities v_{H_2}, v_{HD}, and v_{D_2} (cm s^{-1}) and the gas concentrations (mol cm^{-3}, bracketed) approximate the rates per unit surface area at which those collisions occur. The velocities are calculated as:

$$v_i = \sqrt{\frac{8RT}{\pi M_i}}, \tag{5}$$

where M_i is the molar mass in g mol^{-1} (see Table 4). The rate constants in reactions (R1)–(R3) are the collection of coefficients on the concentration terms; for example $k_{ads,H} = 2v_{H_2}/\Gamma_s^2$.

More recently, a study of HD formation kinetics (Michalak et al., 2012) has suggested that β-PdH does have a measurable activation barrier to dissociative adsorption. However, we anticipate this to be significantly smaller than the surface-to-bulk activation energy, and less likely to be limiting. This activation energy is likely to depend on surface orientation and composition, and is a question worth further investigation in the future. Our simulations included a factor of 2 preceding the velocities in (1)–(3) to capture the fact that each site on a square lattice can be associated with two unique pairs of neighbors. However, we have ignored the fact that gas molecules are not all heading toward the surface at a given time, to which Foltz and Melius attribute a factor of 1/4. Furthermore, it is quite likely that we are ignoring the effects of sticking probabilities or similar mechanistic factors that could modify this coefficient by more than a factor of 2.

2.2. Rate of production of bulk species

The rates of production of the bulk species per unit surface area (mol cm^{-2} s^{-1}) can also be constructed from rate laws:

$$s_{H_b} = \omega_{sb,H} \exp\left(-\frac{E_{diff,H}+E_{abs,H}-E_{ads,H}}{RT}\right)\frac{V_b H_s}{\Gamma_b} - \omega_{bs,H}\exp\left(-\frac{E_{diff,H}}{RT}\right)\frac{V_s H_b}{\Gamma_b}, \tag{6}$$

$$s_{D_b} = \omega_{sb,D} \exp\left(-\frac{E_{diff,D}+E_{abs,D}-E_{ads,D}}{RT}\right)\frac{V_b D_s}{\Gamma_b} - \omega_{bs,D}\exp\left(-\frac{E_{diff,D}}{RT}\right)\frac{V_s D_b}{\Gamma_b}, \tag{7}$$

$$s_{V_b} = -s_{H_b} - s_{D_b}. \tag{8}$$

where Γ_b is the total bulk concentration of filled and vacant sites (mol cm^{-3}) and the bulk vacancy concentration V_b is recovered by:

$$V_b = \Gamma_b - H_b - D_b. \tag{9}$$

The surface-to-bulk transitions, which are the first terms on the right hand sides of (6) and (7), consist of an attempt frequency, a probability that each attempt surmounts the energetic barrier between surface and bulk states, and a concentration of surface species adjacent to a vacant bulk site assuming one bulk site adjacent to each surface site. $E_{abs}-E_{ads}$ is the thermodynamic barrier that must be overcome, and E_{diff} is an additional activation barrier, assumed to be the same as the barrier between adjacent bulk sites. The second term on the right hand side of (6) and (7) is the bulk-to-surface transition, and is similar to the first term, but only the diffusion activation barrier must be overcome. The rate of production of vacant bulk sites is simply the opposite of the sum of those for the two types of occupied sites, because the total number of bulk sites is conserved.

The molar production rates per unit area of the surface species (mol cm^{-2} s^{-1}) are given by a mass balance of the other rates as:

$$s_{H_s} = -2s_{H_2} - s_{H_b} - s_{HD}, \tag{10}$$

$$s_{D_s} = -2s_{D_2} - s_{D_b} - s_{HD}, \tag{11}$$

$$s_{V_s} = -s_{H_s} - s_{D_s}. \tag{12}$$

3. Mathematical model formulation

In an isotope exchange experiment, the solid and gas phases can be either palladium deuteride (PdD) and hydrogen gas (H_2), denoted here as “H to D”, or palladium hydride (PdH) and deuterium gas (D_2) denoted “D to H”. The mathematical formulation is valid for both of these cases. For brevity, we focus mainly on the “H to D” case where H_2 is exchanging isotopes with PdD, but the same general formulation applies to the “D to H” exchange. For this case, the net process is that hydrogen absorbs from the gas into the metal, and a nearly equal amount of deuterium desorbs from the bulk into the gas.

Two models of isotope exchange are developed here. The first model couples hydride diffusion within the solid particle to the surface kinetics, while the second couples the surface kinetics to reactive gas flow in a porous bed. These sections describe the governing equations for the state variables as a function of numerous parameters. Values for those parameters (some of which are determined by additional equations) are discussed in subsequent sections.

3.1. Coupled surface reaction-particle diffusion model

Following the formulation of James et al. (2012), we consider a spherical PdD particle immersed in a rapidly mixed H_2 gas tank. The diffusion of H and D atoms inside a palladium hydride particle is governed by the following partial differential PDEs described in detail elsewhere (James et al., 2012), which include a cross term for the effect of one isotope on the other:

$$\frac{\partial x_H}{\partial t} = \frac{1}{r^2}\frac{\partial}{\partial r}\left[r^2\left(\hat{\mathcal{D}}_{HH}\frac{\partial x_H}{\partial r} + \hat{\mathcal{D}}_{HD}\frac{\partial x_D}{\partial r}\right)\right] \quad \text{in} \quad r \in [0, r_0], \tag{13}$$

$$\frac{\partial x_D}{\partial t} = \frac{1}{r^2}\frac{\partial}{\partial r}\left[r^2\left(\hat{\mathcal{D}}_{DH}\frac{\partial x_H}{\partial r} + \hat{\mathcal{D}}_{DD}\frac{\partial x_D}{\partial r}\right)\right] \quad \text{in} \quad r \in [0, r_0], \tag{14}$$

where $x_H = H_b/\Gamma_b$ and $x_D = D_b/\Gamma_b$. The diffusion coefficients $\hat{\mathcal{D}}_{ij}$ are somewhat complicated, and arise from a detailed consideration of the dependence of chemical potential on concentration for each combination of species. This involves accounting for activated hopping between discrete sites, entropy of mixing, blocking of sites by the opposite isotope, and the fact that the chemical potential increases sharply at high concentrations due to elastic and electronic effects (denoted as the excess chemical potential). The diffusion coefficients are given by:

$$\hat{\mathcal{D}}_{HH} = \hat{\mathcal{D}}_H^E \exp\left(-\frac{E_{diff,H}}{RT}\right)\left(x_H + x_V + \frac{E_{ex}}{RT}x_H x_V\right), \tag{15}$$

$$\hat{\mathcal{D}}_{DD} = \hat{\mathcal{D}}_D^E \exp\left(-\frac{E_{diff,D}}{RT}\right)\left(x_D + x_V + \frac{E_{ex}}{RT}x_D x_V\right), \tag{16}$$

$$\hat{\mathcal{D}}_{HD} = \hat{\mathcal{D}}_{HH} - x_V D_H^E \exp\left(-\frac{E_{diff,H}}{RT}\right), \tag{17}$$

$$\hat{\mathcal{D}}_{DH} = \hat{\mathcal{D}}_{DD} - x_V D_D^E \exp\left(-\frac{E_{diff,D}}{RT}\right), \tag{18}$$

where $x_V = V_b/\Gamma_b$, $\hat{\mathcal{D}}_i^E$ is what the diffusion constant would be in the absence of both activation and the interaction between other H and D species, $E_{diff,i}$ is the activation energy, and E_{ex} is a factor accounting for excess chemical potential. Values for these parameters are provided by James et al. (2012). This diffusion model is easily modified for cylindrical or planar geometries. The PDEs in Eqs. (13) and (14) are subject to the following boundary

conditions:

$$\frac{\partial x_H}{\partial r}(0,t)=0,$$
$$\frac{\partial x_D}{\partial r}(0,t)=0, \tag{19}$$

$$-\left[\hat{\mathcal{D}}_{HH}\frac{\partial x_H}{\partial r}(r_0,t)+\hat{\mathcal{D}}_{HD}\frac{\partial x_D}{\partial r}(r_0,t)\right]=\frac{s_{H_b}}{\Gamma_b},$$
$$-\left[\hat{\mathcal{D}}_{DH}\frac{\partial x_H}{\partial r}(r_0,t)+\hat{\mathcal{D}}_{DD}\frac{\partial x_D}{\partial r}(r_0,t)\right]=\frac{s_{D_b}}{\Gamma_b}. \tag{20}$$

The boundary condition in (20) provides the coupling with the surface reaction model where s_{H_b} and s_{D_b} are calculated by (6) and (7). Moreover, H_s and D_s are given by the following ordinary differential equations (ODE):

$$\frac{dH_s}{dt}=s_{H_s}$$
$$\frac{dD_s}{dt}=s_{D_s} \tag{21}$$

where s_{H_s} and s_{D_s} are given by (10) and (11), respectively.

Careful attention to initial conditions to ensure that they are physically realistic can allow a numerical simulation to proceed efficiently. All species are assumed to be in chemical equilibrium at the start of the experiment, before a change is imposed. The outside tank is assumed rapidly stirred with a large supply of gas, so that the gas concentrations are instantaneously controllable in the experiment. The molar gas concentrations are related by:

$$[C]=\frac{P}{RT}=[H_2]+[D_2]+[HD]. \tag{22}$$

where P is the constant outside pressure. The gas is initially H_2 such that:

$$[H_2]=\mathcal{C}\frac{P}{RT}, \tag{23}$$

where $\mathcal{C}$ is a constant near unity, and brackets denote a gas-phase concentration. All gas concentrations must remain sufficiently above zero to avoid going negative when finite time steps are taken during a simulation, so it is best to not force any gas concentrations to zero or to the total concentration P/RT. To accomplish this, a maximum purity $\mathcal{C}$ is used (James et al., 2012). We arbitrarily chose $\mathcal{C}=0.98$; to model a specific experiment, a better choice would reflect the isotopic purity of the gas used. When at equilibrium, as is assumed at the start of the experiment, $[H_2]$, $[D_2]$, and [HD] are related by the equilibrium relationship:

$$[D_2]=\frac{[HD]^2}{K_{HD}[H_2]}, \tag{24}$$

where K_{HD} is the equilibrium constant of reaction (R7) defined in Section 4.1.4. To allow the simulation to make time steps faster than the time scale of changes of boundary conditions, $[H_2]$ is linearly ramped from $0.01P/RT$ up to $\mathcal{C}P/RT$ over a time scale much shorter than that of the simulation. In the same time, $[D_2]$ is linearly ramped from $\mathcal{C}P/RT$ down to $0.01P/RT$.

Initially, the particle is mostly composed of PdD:

$$H_b(r,0)=\mathcal{Z}\Gamma_b,$$
$$D_b(r,0)=\ell\Gamma_b,$$
$$H_s=\mathcal{Z}\Gamma_s,$$
$$D_s=\mathcal{C}\Gamma_s. \tag{25}$$

Realistic estimates of the initial hydrogen loading $\mathcal{Z}$ and the initial deuterium loading ℓ are best obtained from the experimentally known equilibrium constants for (R6)–(R8), as defined in Section 4. A nonlinear system of equations formed by these and (24) can be solved to obtain $\mathcal{Z}$ and ℓ as follows:

$$\ell=(1-\mathcal{Z}-\ell)\sqrt{\ell([C]-[H_2]-[HD])K_{abs,D}},$$
$$\mathcal{Z}=(1-\mathcal{Z}-\ell)\sqrt{\ell[H_2]K_{abs,H}}, \tag{26}$$

where $K_{abs,H}$ and $K_{abs,D}$ are the equilibrium constants of reactions (R6) and (R8), respectively, defined in Section 4.1.4. To complete the solution, $H_b=\mathcal{Z}\Gamma_b$ then $V_b=\Gamma_b(1-\mathcal{Z})-D_b$.

3.2. Coupled surface reaction-gas flow model

For a packed powder bed, we assume that gas flow depends on the microscopic dimensions of the void volume rather than the macroscopic position in the radial direction, and that the effect of microscopic variations of void geometry is smoothed out by rapid mixing of gases on that length scale. Under these conditions, it is reasonable to model the powder bed with a one-dimensional geometry that contains no radial variation. We further assume that the temperature is constant everywhere, which is plausible if the bed radius is sufficiently small (length/radius >10), and the thermal conductivities and heat capacities of the powder and walls are sufficiently high. In this model, we assume that concentrations inside a particle are uniform, to allow the problem to be simplified. In practice, we can first use the particle model to verify that this assumption is appropriate. The following set of PDEs are applied, starting with a form of Darcy's law to provide a semi-empirical relationship between pressure and flow (Kanouff et al., 2013):

$$u=-\frac{\kappa}{\mu}\frac{\partial P}{\partial z}, \tag{27}$$

where u (cm s^{-1}) is the superficial gas velocity (so that u=moles per second at entrance or exit, divided by concentration and bed cross-sectional area), z (cm) is the spatial coordinate, μ (Pa.s) is the viscosity of the gas mixture, and κ (cm^2) is the permeability of the powder bed. The overall mass conservation equation describes that the local change of gas concentration with time is the result of the gradient of flow (the advective term) and chemical reaction. This equation accounts for the fact that the gas exists only in the pore spaces between particles.

$$\frac{\partial(\rho\phi)}{\partial t}+\frac{\partial(\rho u)}{\partial z}=S_A\sum_{i=H_2,D_2,HD}s_iM_i \quad \text{in} \quad z\in[0,L], \tag{28}$$

where L is the reactor axial length (cm), S_A is the surface area per unit of bed volume (cm^2 cm^{-3}), and ϕ is the bed porosity (cm^3 cm^{-3}). The gas density ρ (g cm^{-3}) is calculated by mole-based averaging as:

$$\rho=\sum_{i=H_2,D_2,HD}[i]M_i. \tag{29}$$

The molar conservation law for each species also includes a term accounting for gas phase diffusion.

$$\frac{\partial(\phi[H_2])}{\partial t}+\frac{\partial}{\partial z}([H_2]u)-\frac{\partial}{\partial z}\left[[C]\tilde{\mathcal{D}}^*\frac{\partial}{\partial z}\left(\frac{[H_2]}{[C]}\right)\right]=S_As_{H_2} \quad \text{in} \quad z\in[0,L],$$
$$\frac{\partial(\phi[D_2])}{\partial t}+\frac{\partial}{\partial z}([D_2]u)-\frac{\partial}{\partial z}\left[[C]\tilde{\mathcal{D}}^*\frac{\partial}{\partial z}\left(\frac{[D_2]}{[C]}\right)\right]=S_As_{D_2} \quad \text{in} \quad z\in[0,L], \tag{30}$$

where $\tilde{\mathcal{D}}^*$ is the effective diffusion constant for the gas mixture discussed further in Section 4.2. The concentration of [HD] is recovered as:

$$[HD]=[C]-[H_2]-[D_2] \tag{31}$$

The conservation equations for the separate species in Eq. (30) are consistent with the mass conservation equation in Eq. (28). By

summing the equations in (30) and accounting for the constraint in Eq. (31), the diffusion terms are cancelled and (28) is recovered (Chen et al., 2006). The gas flow problem is quite complex, and numerous other transport phenomena could be considered. These include molecular (Knudsen) flow when void spaces are small and pressure is low; inertial (Forchheimer) contributions when velocities are high; thermal diffusion when thermal gradients are present; the Ergun equation for a certain range of Reynolds numbers; and dispersive mixing, especially when flow paths are heterogeneous. Careful design of experiments should minimize the effects of these phenomena, which are neglected in this model for the sake of simplicity. The diffusion term [third term on the left-hand side of (30)] has a small contribution compared to the advection term in isotope exchanges except at low gas flow rates. However, it is included when solving the PDEs because it provides a smoothing effect to the solution and minimizes the numerical challenges (*e.g.*, oscillations, negative concentrations, etc.) encountered in nonlinear and purely hyperbolic equations (Evans, 2010).

Because the source terms s_i depend on the surface and bulk concentrations, differential equations must be solved to determine each of these. The surface concentrations are governed by the ODEs in (21). For the bulk species, we assume that their concentrations are constant within each particle in the bed. This assumption is valid if the transport within the hydride particle is limited by the surface reaction at the particle gas interface (*e.g.* for small enough particles). In Section 6.1, we will show that the assumption can be useful over a wide range of conditions. Furthermore, accounting for the variations of the bulk concentration in the particles in this case makes the model much more computationally cumbersome, as mentioned in the introduction. Following this assumption, the bulk species are governed by the following ODEs:

$$\frac{\mathrm{dH}_b}{\mathrm{d}t}=\frac{S_A s_{\mathrm{H}_b}}{1-\phi},$$
$$\frac{\mathrm{dD}_b}{\mathrm{d}t}=\frac{S_A s_{\mathrm{D}_b}}{1-\phi}, \tag{32}$$

where the coefficients on the source terms convert surface area to solid volume. V_b and V_s are computed by (9) and (4), respectively.

The initial conditions can be found by assuming that at $t=0$, the mass sources are negligible and the pressure is at steady state (Shugard and Robinson, 2014). For constant gas transport properties and temperature, and ideal gases, (28) reduces to

$$\frac{\partial}{\partial z}\left(P\frac{\partial P}{\partial z}\right)=0. \tag{33}$$

where z is the axial coordinate in the direction of flow. With initial upstream and downstream pressures, P_1 and P_2, the initial pressure field is given by:

$$P_f=(P_1+P_2)/2 \tag{34}$$

Initially, the bed is composed of almost all PdD, so at $t=0$, the concentrations are the one given in Table 1, where $\mathcal{Z}$, $\mathcal{C}$, and ℓ are chosen in the same way as for the particle model. The boundary pressures and flow rate are obtained based on experimental data (Kanouff et al., 2013). When the bed is connected to supply and receiver tanks of equal volume V_t, the pressure at the bed inlet $P(0,t)$ is the same as the supply tank pressure, and the concentrations are:

$$[\mathrm{H}_2](0,t)=\mathcal{C}\frac{P(0,t)}{RT},$$
$$[\mathrm{D}_2](0,t)=[\mathrm{HD}](0,t)=\mathcal{Z}\frac{P(0,t)}{RT}, \tag{35}$$

An approximate but realistic pressure profile in this case is given by an exponentially decaying function with a time constant α such that the final pressure in the bed is equal to P_f. This choice should facilitate comparison to experimental data, where the inlet and outlet pressures are typically recorded; implementations of other arrangements such as differing tank volumes or constant flow rates would be straightforward. Thus, the inlet and outlet pressures are:

$$P(0,t)=P_1-\frac{P_1-P_2}{2}\left(1-e^{-t/\alpha}\right),$$
$$P(L,t)=P_2+\frac{P_1-P_2}{2}\left(1-e^{-t/\alpha}\right). \tag{36}$$

These expressions can also be thought of as the solutions of a first order ODE that follow from a combination of Darcy's law and a conservation law (Shugard and Robinson, 2014). The exponential pressure profile neglects the initial compression of gas in the bed to obtain a steady-state pressure profile, and also neglects the fact that slightly more hydrogen than deuterium is stored in the solid at a given pressure. These omissions are justifiable if the tanks contain at least several times more hydrogen and/or deuterium than is stored in the solid, and much more volume than the void volume in the bed. To ensure that the simulation algorithm can perform a sufficient number of timesteps during the initial pressurization of the bed, we initially ramp the pressures over a time much shorter than the total simulation time from P_f to the values in Eq. (36) evaluated for $t=0$. In Section 4.3, the bed permeability, κ, is calculated as a function of α, which is assumed to be more easily derived from experimental data. At the bed outlet, the following outflow boundary conditions on the gas concentrations are imposed:

$$\frac{\partial}{\partial z}\left(\frac{[\mathrm{H}_2]}{[\mathrm{C}]}\right)=0,$$
$$\frac{\partial}{\partial z}\left(\frac{[\mathrm{D}_2]}{[\mathrm{C}]}\right)=0, \tag{37}$$

which also accounts for the fact that the gas exiting the bed is a mixture of total concentration [C].

Table 1
Porous bed and hydride particles properties at $T=20$ °C.

	H	D
Bulk	$\mathcal{Z}\Gamma_b$	$\ell\Gamma_b$
Surface	$\mathcal{Z}\Gamma_s$	$\mathcal{C}\Gamma_s$
Gas	$\mathcal{Z}P_f/RT$	$\mathcal{C}P_f/RT$

4. Chemical and physical parameters

Many of the parameters in the equations above can be estimated from independent information. Doing so can provide a starting point for more direct and detailed comparisons to isotope exchange experiments.

4.1. Surface kinetics parameters

4.1.1. Site concentrations

The number of surface and bulk sites can be estimated by assuming that there is one vacancy per Pd atom. The β-phase palladium hydride is face-centered cubic (FCC) with a lattice parameter of 0.404 nm (Flanagan and Oates, 1991), varying by about 1% as a function of hydrogen content and over the temperature range studied here (Abbensetht and Wipf, 1980). There are 4 atoms in an FCC unit cell. The volume of a mole of unit cells is $N_A a^3$, where N_A is Avogadro's number (6.023×10^{23} mol^{-1}). Γ_b is then $\frac{4}{N_A a^3}$ or 0.101 mol cm^{-3} for β-phase PdH. In practical applications, the initial bulk isotope loading, ℓ, is always less than unity

and its value depends on the equilibrium state of the system. Based on (26), $\ell = 0.88$ at T=-60 °C and 0.81 at T=20 °C.

The (1 0 0) surface of an FCC lattice contains two atoms, so the analogous calculation for Γ_s is then $\frac{2}{N_A a^2}$. As noted previously, a given crystal face may have multiple types of adsorption site with different energies, as would different crystal faces, boundaries between crystals, and defects within them. The approach implemented here results in the same Γ_b as calculated by Ward and Dao (1999), but their value for $\Gamma_s = 2.04 \times 10^{-9}$ mol cm^{-2} differs slightly because it uses a generic calculation that makes no assumption about surface structure. From the number of atoms per unit volume, they extract an atomic length scale $\lambda = (N_A \Gamma_b)^{-1/3}$, and then construct $\Gamma_s = \left(N_A \lambda^2\right)^{-1}$, the reciprocal of the area occupied by a mole of atoms defined by this length scale. The resulting Γ_s is higher by a factor of $2^{1/3}$ which yields 2.56×10^{-9} mol cm^{-2} for PdH. In this study, we used $\Gamma_s = 2.56 \times 10^{-9}$ mol cm^{-2} for all the calculations except for the calculation of the desorption attempt frequency where we used 2.04×10^{-9} mol cm^{-2} (see Section 4.1.3 below). The initial isotope loading is calculated as $\ell = 0.81$ (see Eq. (26)).

4.1.2. Activation energy components

The surface-to-bulk activation energy depends on the thermodynamic stability of surface sites, which is quite sensitive to the atomic-scale geometry and composition of the surface. For α-Pd, Ward and Dao (1999) note a wide range of possible values for $E_{ads,H}$, but use values between -42 and -50 kJ·(mol H)$^{-1}$. Conrad et al. (1974) report that $E_{ads,D}$ is 3.4 kJ (mol D)$^{-1}$ lower than $E_{ads,H}$. Powell and Kirkpatrick (1991) reported a value equivalent to -42 kJ (mol H)$^{-1}$ for α-PdH by studying hydrogen uptake by a Pd sphere. In contrast, Rayhel et al. (2011) reported activation energies equivalent to values between -15 and -18 kJ·(mol H)$^{-1}$, from NMR measurements of exchange of H between the gas phase and β-PdH, which could plausibly be assumed to be limited by the surface-to-bulk step. Michalak et al. (2012) ignore the difference between $E_{ads,H}$ and $E_{ads,D}$. This and other reports (Bennett and Fuggle, 1982; Johansson et al., 2010) claim that the $E_{ads,H}$ values for β-PdH are smaller in magnitude than -20 kJ·(mol H)$^{-1}$. In this study, we acknowledge that these parameters are likely to depend on composition and structure of the surface (Jewell and Davis, 2006), and consider them to be adjustable both in the model and in experimental conditions, spanning much of the range of reported values. It would be more realistic to consider a distribution of simultaneous values. However, for convenience, a single value is implemented for a given simulation. The difference between $E_{ads,H}$ and $E_{ads,D}$ is fixed at the corresponding difference between $E_{abs,H}$ and $E_{abs,D}$ (discussed below), which is slightly smaller than the value used by Conrad et al. (1974). For $E_{ads,HD}$, the sum $E_{ads,H} + E_{ads,D}$ can be used, minus the enthalpy of formation per mole of HD (0.325 kJ (mol HD)$^{-1}$) (Larson et al., 2011). Values for E_{abs} for β-phase PdH and PdD are obtained from Larson et al. (2011), drawing from the work of Charton et al. (1999) and Santandrea and Behrens (1986). They depend on the number of occupied sites due to the elastic and electronic effects discussed earlier.

$$-2E_{abs,H} = 100.35 - 90.04(x_H + x_D) \quad [kJ \cdot (molH)^{-1}],$$
$$-2E_{abs,D} = 95.53 - 90.04(x_H + x_D) \quad [kJ \cdot (mol\,D)^{-1}], \tag{38}$$

where x_H and x_D are stoichiometric coefficients representing the number of H and D atoms per Pd atom, respectively.

The diffusion activation energies reported by Flanagan and Oates (1991) and Ward and Dao (1999) are similar, but Flanagan and Oates (1991) present data for each isotope at lower temperatures than Ward and Dao (1999) and their values were derived for α-PdH. More appropriate values for the β-PdH phase are found in the study of James et al. (2012). $E_{diff,H}$ is equal to 26.04 kJ·(mol H)$^{-1}$ and $E_{diff,D}$ is equal to 28.18 kJ·(mol D)$^{-1}$. Excess chemical potential, E_{ex}, is found by differentiating E_{abs} with respect to either x_H or x_D yielding $E_{ex} = 45$ kJ mol^{-1}. Further details on the derivation of the excess chemical potential are found in the study of James et al. (2012).

4.1.3. Attempt frequencies

Attempt frequencies for H_s and H_b reactants were estimated by Ward and Dao (1999). From experimental data on thermal desorption at low coverage, they report an exponential prefactor for desorption $k_0 = 4.8 \times 10^{21}$ cm^2 mol^{-1} s^{-1}. This can be converted into an attempt frequency by multiplying by Γ_s. Because desorption involves collisions between neighboring surface atoms spaced by a distance scaling with the lattice parameter, we use our value of $\Gamma_s = 2.04 \times 10^{-9}$ mol cm^{-2} for β-PdH. This results in $\omega_{des,H} = 9.8$ THz. Attempt frequencies can be assumed to vary by $M^{-1/2}$, so $\omega_{des,D} = 6.9$ THz is lower by a factor of 0.71.

From bulk diffusion data, Ward and Dao (1999) converted an experimentally derived diffusion constant prefactor $\hat{\mathcal{D}}^E$ into a jump frequency between bulk sites by assuming a diffusion distance of one lattice parameter, and 12 neighboring octahedral sites within the FCC lattice, leading to a diffusion attempt frequency of $\omega_{diff} = 12\hat{\mathcal{D}}^E / a^2 = 23$ THz (Ward and Dao, 1999, Eq. 21) This jump frequency is preferably derived using the values from James et al. (2012) of $\hat{\mathcal{D}}^E_H = 5.470 \times 10^{-2}$ cm^2 s^{-1} and $\hat{\mathcal{D}}^E_D = 2.103 \times 10^{-2}$ cm^2 s^{-1}. Using a β-PdH lattice parameter of 0.404 nm, this yields jump frequencies of $\omega_{des,H} = 40.26$ and $\omega_{des,D} = 15.46$ THz.

The surface-to-bulk attempt frequencies $\omega_{bs,H}$ and $\omega_{bs,D}$ are assumed to involve similar jumps to those for diffusion, but in a specific direction instead of to all 12 neighbors. Ward and Dao (1999) use a factor of 1/3 because one third of the jumps from the (0 0 1) plane will be to the next (0 0 1) plane; this results in $\omega_{bs,H} = 13.42$ THz and $\omega_{bs,D} = 5.15$ THz.

4.1.4. Relationships between attempt frequencies and equilibrium constants

Several other attempt frequencies are needed, for which straightforward experimental measurements are not available. However, they can be derived indirectly by considering relationships among these factors at equilibrium. This assumes that each reaction (or any combination of them) is also at equilibrium, and hence the forward and reverse reaction rates must be equal. For example, when (R1) is at equilibrium, the rate at which H_2 and surface vacancies combine to form two surface hydrides must equal the rate at which two surface hydrides form H_2 and two vacancies; by setting $s_{H_2} = 0$ in (1):

$$2\nu_{H_2}\left(\frac{V_s}{\Gamma_s}\right)^2 [H_2] = \omega_{des,H} \exp\left(\frac{2E_{ads,H}}{RT}\right)\frac{H_s^2}{\Gamma_s}. \tag{39}$$

Rearranging this equation yields:

$$K_{R1} = \frac{k_{ads,H}}{k_{des,H}} = \frac{H_s^2}{[H_2]V_s^2} = \frac{\nu_{H_2}}{\omega_{des,H}\Gamma_s}\exp\left(-\frac{2E_{ads,H}}{RT}\right). \tag{40}$$

The preceding equation is only useful if the equilibrium constants, K_i, are known independently, which is true for a few combined reactions. The attempt frequency for recombinative desorption of HD is an otherwise elusive parameter that can be eliminated by this approach. Larson et al. (2011) note that the reaction [R7] is equivalent to (R1) + (R3) − 2(R2) (see Section 2), so

that:

$$K_{HD} = \frac{K_{R1}K_{R3}}{K_{R2}^2}, \tag{41}$$

where K_{HD} is the unitless equilibrium constant for (R7). The preceding equation can be rearranged to:

$$k_{des,H} = k_{ads,H}\left(\frac{k_{des,H}k_{des,D}K_{HD}}{k_{ads,H}k_{ads,D}}\right)^{1/2}. \tag{42}$$

Substituting the definition of each rate constant as apparent from the rate laws for s_i from (1)–(3) results in an expression for the recombinative desorption frequency of HD:

$$\omega_{des,HD} = \nu_{HD}\exp\left(-\frac{E_{ads,HD}-E_{ads,H}-E_{ads,D}}{RT}\right)\left(\frac{\omega_{des,H}\omega_{des,D}K_{HD}}{\nu_{H_2}\nu_{D_2}}\right)^{1/2}. \tag{43}$$

K_{HD} is provided by Larson et al. (2011, Eq. 11) and Foltz and Melius (1987, Eq. 15) as:

$$K_{HD} = 4.242\exp\left(-\frac{2E_{HD}}{RT}\right), \tag{44}$$

where the numerator inside the exponential is the enthalpy of reaction (R7), which forms two HD molecules. Larson et al. (2011) used a similar approach to eliminate the bulk-to-surface attempt frequencies ω_{bs} by making use of the known equilibrium constants for the reactions between gas- and bulk-phase hydrogen and deuterium, (R6)–(R8). There are relatively reliable ways to estimate ω_{bs} from experimental data, as demonstrated above. The surface-to-bulk attempt frequencies ω_{sb} are less well documented, so the following equilibrium constants are used to eliminate them instead. Because the hydrogen gas-bulk reaction (R6)=(R1)+2 (R4) is the sum of the gas-surface and two surface-bulk reactions, $K_{abs,H} = K_{R6} = K_{R1}K_{R4}^2$, where $K_{abs,H}$ ($cm^3\ mol^{-1}$) is the equilibrium constant for (R6). This leads to a surface-to-bulk rate constant:

$$k_{sb,H} = k_{bs,H}\left(\frac{k_{des,H}K_{abs,H}}{k_{ads,H}}\right)^{1/2}. \tag{45}$$

Substitutions of the rate constant definitions yield:

$$\omega_{sb,H} = \omega_{bs,H}\exp\left(\frac{E_{ads,H}}{RT}\right)\left(\frac{\omega_{des,H}K_{abs,H}\Gamma_s}{2\nu_{H_2}}\right)^{1/2}, \tag{46}$$

where $K_{abs,H}$ is given by Larson et al. (2011) as (note that the units on the prefactor are $cm^3\ mol^{-1}\ K^{-1}$):

$$K_{abs,H} = 2.050\times10^{-4}T\exp\left(-\frac{2E_{abs,H}}{RT}\right). \tag{47}$$

A similar analysis for the deuterium reactions results in Larson et al. (2011) (note again that the units on $K_{abs,H}$ are $cm^3\ mol^{-1}\ K^{-1}$):

$$\omega_{sb,D} = \omega_{bs,D}\exp\left(\frac{E_{ads,D}}{RT}\right)\left(\frac{\omega_{des,D}K_{abs,D}\Gamma_s}{2\nu_{D_2}}\right)^{1/2}, \tag{48}$$

$$K_{abs,D} = 2.265\times10^{-4}T\exp\left(-\frac{2E_{abs,D}}{RT}\right). \tag{49}$$

Table 2 summarizes the parameter values for the attempt frequencies, rate laws, and activation energies with the expressions used to compute them. Table 2 also includes the diffusion coefficients used in the coupled surface reaction-particle diffusion model (see Section 3.1). Table 3 summarizes the reaction kinetics model parameters and variables when $x_H+x_D=0.7$, $E_{ads,H} = -25\ kJ\cdot(mol\ H)^{-1}$ and for T=20 °C and T=-60 °C. Expressions for $\omega_{des,HD}$, $\omega_{sb,H}$, and $\omega_{sb,D}$ could be proposed that are based on a more intuitive molecular mechanism, but this could lead to less realistic results, because the equilibrium relations must be satisfied somehow. We instead proceed without attempting to divine a mechanistic interpretation of Eqs. (43), (46) and (48).

Table 3
Reaction kinetics model parameters and variables for $x_H+x_D=0.7$, $E_{ads,H} = -25\ kJ\cdot(mol\ H)^{-1}$ and for T=20 °C and T=-60 °C (in parentheses).

	H value	D value
ω_{sb} (THz)	0.092 (0.03)	0.0051 (0.00085)
K_{abs} ($cm^3\ mol^{-1}$)	2.7×10^5 (6.2×10^7)	4.13×10^4 (4.51×10^6)
ν ($cm\ s^{-1}$)	1.76×10^5 (1.5×10^5)	1.24×10^5 (1.06×10^5)
E_{abs} ($kJ\cdot(mol\ H\ or\ D)^{-1}$)	−18.7	−16.25
$\omega_{des,HD}$ (THz)	16.23 (12.65)	
ν_{HD} ($cm\ s^{-1}$)	1.43×10^5 (1.23×10^5)	
K_{HD}	3.25 (2.94)	
$E_{ads,HD}$ ($kJ\cdot(mol\ HD)^{-1}$)	−52.7	
$E_{ads,D}$ ($kJ\cdot(mol\ D)^{-1}$)	−27.4	

Table 2
Reaction kinetics model parameters and variables.

	H value	D value
ω_{bs} (THz)	13.42	5.15
ω_{des} (THz)	9.8	6.9
ω_{sb} (THz)	$\omega_{bs,H}\exp\left(\frac{E_{ads,H}}{RT}\right)\left(\frac{\omega_{des,H}K_{abs,H}\Gamma_s}{\nu_{H_2}}\right)^{1/2}$	$\omega_{bs,D}\exp\left(\frac{E_{ads,D}}{RT}\right)\left(\frac{\omega_{des,D}K_{abs,D}\Gamma_s}{\nu_{D_2}}\right)^{1/2}$
$-2E_{abs}$ ($kJ\cdot(mol\ H\ or\ D)^{-1}$)	$100.35-90.04(x_H+x_D)$	$95.53-90.04(x_H+x_D)$
E_{diff} ($kJ\cdot(mol\ H\ or\ D)^{-1}$)	26.04	28.18
E_{ads} ($kJ\cdot(mol\ H\ or\ D)^{-1}$)	−35 to −20	$E_{ads,H}+2.41$
K_{abs} ($cm^3\cdot mol^{-1}$)	$2.05\times10^{-4}T\exp\left(-\frac{2E_{abs,H}}{RT}\right)$	$2.265\times10^{-4}T\exp\left(-\frac{2E_{abs,D}}{RT}\right)$
ν ($cm\ s^{-1}$)	$\sqrt{8RT/\pi M_{H_2}}$	$\sqrt{8RT/\pi M_{D_2}}$
$\hat{\mathcal{D}}^E$ ($cm^2\ s^{-1}$)	5.47×10^{-3}	2.103×10^{-2}
$\omega_{des,HD}$ (THz)	$\nu_{HD}\exp\left(-\frac{E_{ads,HD}-E_{ads,H}-E_{ads,D}}{RT}\right)\left(\frac{\omega_{des,H}\omega_{des,D}K_{HD}}{\nu_{H_2}\nu_{D_2}}\right)^{1/2}$	
ν_{HD} ($cm\ s^{-1}$)	$\sqrt{8RT/\pi M_{HD}}$	
E_{ex} ($kJ\ mol^{-1}$)	45	
E_{HD} ($kJ\cdot(mol\ HD)^{-1}$)	0.3245	
K_{HD}	$4.242\exp\left(-\frac{2E_{HD}}{RT}\right)$	
$E_{ads,HD}$ ($kJ\cdot(mol\ HD)^{-1}$)	$E_{ads,H}+E_{ads,D}-E_{HD}$	

4.2. Gas transport parameters

The gas viscosity is temperature and composition dependent. It is given by White (2006):

$$\mu = \left(\frac{T[K]}{273}\right)^{0.68} \sum_{i=H_2,D_2,HD} \frac{\mu_i[i]}{[C]}, \tag{50}$$

where μ_i is the viscosity of each gas species at 273 K. The gas diffusivities are also assumed to be temperature and composition dependent (Anthony, 2001):

$$\tilde{\mathcal{D}}_i = \left(\frac{T[K]}{400}\right)^{1.667} \left(\frac{1.01\times 10^5}{P}\right) \sum_{i=H_2,D_2,HD} \frac{\tilde{\mathcal{D}}_{0,i}[i]}{[C]}. \tag{51}$$

The viscosity μ_i and diffusivity $\tilde{\mathcal{D}}_{0,i}$ for D_2 and HD were deduced from those for H_2 by assuming that $\mu_i = \mu_{H_2}\sqrt{M_i/M_{H_2}}$ and $\tilde{\mathcal{D}}_{0,i} = \tilde{\mathcal{D}}_{0,H_2}\sqrt{M_{H_2}/M_i}$. The effective diffusivity $\tilde{\mathcal{D}}^*$ for the gas mixture is computed as the weighted average (Dullien, 1979; Kanouff et al., 2013):

$$\tilde{\mathcal{D}}^* = \frac{\sum_{i=H_2,D_2,HD}\tilde{\mathcal{D}}_i[i]/[C]}{\tau}, \tag{52}$$

where $\tilde{\mathcal{D}}_i$ is the pure gas diffusivity and τ is the bed tortuosity. $\tilde{\mathcal{D}}^*$ accounts for the decrease in the diffusivity due to the bed tortuosity. In Eq. (52), we divide the gas diffusivity by the tortuosity according to the formula in Dullien (1979) (Eq. 7.3.6, page 346) for unsteady-state diffusion. The tortuosity was estimated based on the bed porosity as $1.25/\phi^{1.1}$ (Shugard et al., 2014) (see Table 5). The gas transport parameters are summarized in Table 4.

4.3. Particle and bed properties

For spherical particles, the surface area per total volume $S_A = 3(1-\phi)/r_0$. If the particles are loosely packed, ϕ may be set to 0.75. For $r_0 = 1$ μm particles, we obtain $S_A = 7500$ cm^2/cm^3.

The bed permeability is estimated with Darcy's equation, (27), as a function of the initial inlet and outlet pressures, and the decay time constant, α (see (36)). H_2 gas supply and receiver tanks of volume V_t are connected to the bed of length L and cross-sectional area A_b. The numbers of moles in the supply tank and receiver are equal to:

$$n_1(0,t) = \frac{P_1(0,t)V_t}{RT}, n_2(0,t) = \frac{P_2(0,t)V_t}{RT}. \tag{53}$$

The inlet gas velocity is obtained by dividing $dn(0,t)/dt$ by $[C]A_b$. Furthermore, by assuming that this molar flow rate and the bed permeability κ are constant throughout the bed, Darcy's law can be applied on the whole bed to derive the following expression of κ:

$$\kappa = \frac{\mu_{H_2} L V_t}{\alpha A_b (P_1 + P_2)}. \tag{54}$$

The values of these parameters are listed in Table 5.

Table 4
Gas species transport parameters (Anthony, 2001; White, 2006).

	H_2	D_2	HD
M_i (g mol^{-1})	2	4	3
μ_i (Pa.s^{-1})	0.835×10^{-5}	1.181×10^{-5}	1.023×10^{-5}
$\mathcal{D}_{0,i}$ (cm^2 s^{-1})	1.71	1.21	1.39

Table 5
Bed physical properties.

P_1	P_2	α	L	V_t	A_b	κ	τ
379.21 kPa	34.47 kPa	66 s	2 cm	23 cm^3	3.14 mm^2	4.5×10^{-10} cm^2	1.71

5. Numerical implementation

The governing equations described above were solved using the Matlab interface of the commercial finite element software, COMSOL 4.2a. The equations can also be solved using any other PDE finite element solver. In the coupled surface reaction-particle diffusion model, the fine one-dimensional mesh elements inside the spherical particle are second-order. The total number of elements is 2,500 with 20,018 corresponding degrees of freedom. In the coupled surface reaction-gas flow model, the fine one-dimensional mesh elements inside the bed are also second-order for improved accuracy in the reaction region. For a bed length of $L=2$ cm, the total number of elements is 2,500 such that the total number of degrees of freedom is 35,250. Because the flow model is highly nonlinear and dominated by advection, the fine mesh was required to prevent numerical instabilities that could lead to negative concentrations. For both models, the mesh sensitivity was checked by halving the mesh size and verifying that there is a negligible change in the results. The gas species mass balance was also verified for consistency. An implicit scheme was used to integrate the transient system of PDEs and ODEs (*i.e.*, Eqs. (13), (14), and (27)–(30)).

6. Results

Parametric studies were conducted, focusing attention on two important parameters: the operating temperature, T, and the hydrogen surface adsorption energy, $E_{ads,H}$, which is tightly related to the state of the palladium hydride gas-solid surface. The range of $E_{ads,H}$ interrogated is one that incurs a moderately fast reaction, namely $-35 \le E_{ads,H} \le -20$ kJ·(mol H)$^{-1}$. It falls around the lower range of measured values reported in the literature, as noted in Section 4.1.2.

6.1. Coupled surface reaction-particle diffusion model

The response of a spherical hydride particle to an abrupt change in the composition of its gas environment informs us whether the transport rate is limited by bulk diffusion of hydride species or surface reaction kinetics. Fig. 3 shows the temporal evolution of the bulk species fractions at the particle center ($r=0$, solid curves) and surface ($r=r_0$, dashed curves) at two different temperatures.

At early times, the plots imply that the isotope initially contained in the particle is unilaterally exchanging with vacancies before it exchanges with the opposite isotope, as shown by the variation in vacancy concentration at around 10^{-2} (red curves in Fig. 3, top right). This is mainly due to the slightly imbalanced choices of $\mathcal{Z}$, ℓ, and $\mathcal{C}$ as initial conditions [see (25)] and to the fact that outside gas concentrations are quickly ramped in time as described in Section 3.1. At later times, the mole fraction of vacancies is about 31% and 38% for the “H to D” and “D to H”,

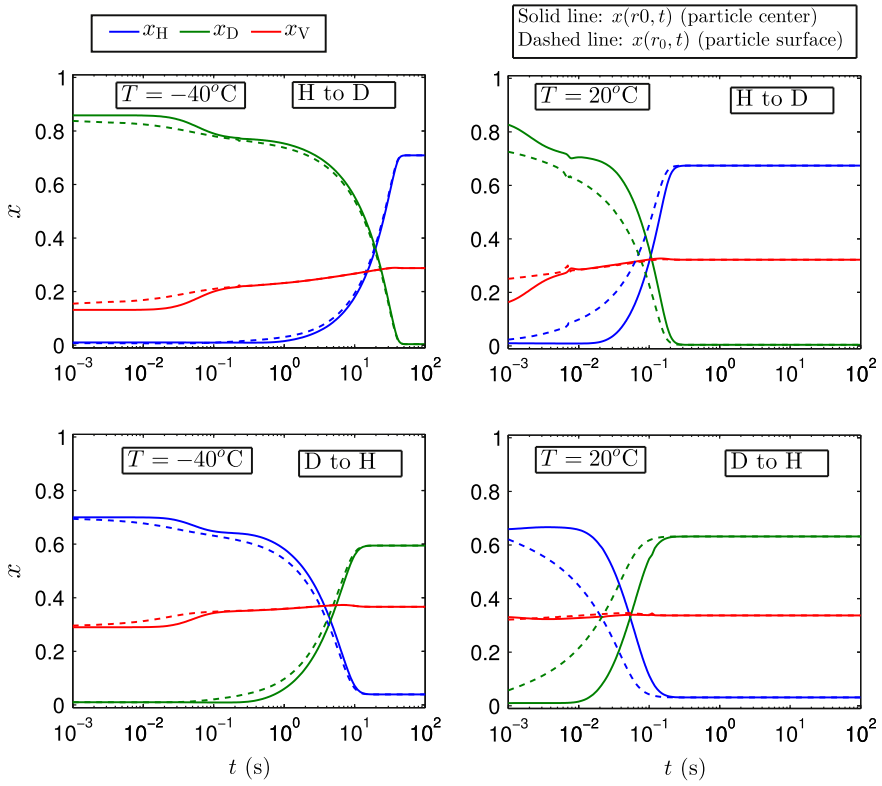

Fig. 3. Temporal variation of the bulk species mole fraction in a hydride particle at the particle center (solid lines) and surface (dashed lines) for the: (top row) "H to D" and (bottom row) "D to H" exchanges. The results are generated using the coupled surface reaction-particle diffusion model with a spherical particle of radius $r_0 = 1$ μm and a local pressure P=100 kPa for $E_{ads,H} = -22.59$ kJ · (mol H)$^{-1}$ and two different temperatures, as indicated.

respectively, varying slightly with temperature and isotopic composition, as expected (Flanagan and Oates, 1991).

The time at which the dotted curves for H and D cross is indicative of the timescale of the surface reaction. It is slightly faster for the "D to H" case because, as formulated here, the surface-to-bulk activation energy is lower for D than for H. This is a result of the composition-dependent absorption enthalpy, and the assumption that the activation energy depends on the absorption enthalpy.

Differences in the times when the H and D curves cross between the dashed curve (particle surface) and solid curve (particle center) is an indication of slow diffusion relative to the surface reaction. If the crossover time for the dashed curve is close to that of the solid curves (*e.g.*, at T=-40 °C), the transport of H and D through the surface is about the same as the bulk diffusion. Conversely, at 20 °C the larger difference between the solid and dashed lines indicates that the concentrations at the particle center and surface evolve at different rates. This means that there is a concentration gradient within the particle during the exchange, demonstrating the significant effect of diffusion. Therefore, diffusion limits the overall exchange at T=20 °C. This effect of diffusion-limited exchange rates can also be observed by plotting the radial concentration distribution. Fig. 4 shows that at lower temperatures, the concentration inside the particle is nearly constant over the course of the isotope exchange, making the predictions of the bulk diffusion model redundant to the evaluation of the concentration at the particle surface (*i.e.*, diffusion is not limiting and need not be considered at low temperatures at this particle radius). On the other hand, the concentration profile at high temperatures exhibits early-time gradients between the particle center and surface, which implies that in such cases it is important to account for the bulk diffusion for an accurate prediction of the isotope exchange dynamics.

When simulating models that involve both surface and bulk transport phenomena, it is important to understand the interplay between these two transport modes. For example, when modeling reactive gas flows in powder beds, it is crucial to know beforehand whether the diffusion rates of the species inside the solid particles is negligible. This would be the case if the transport regime is limited by the surface reaction rate at the solid-gas interface. A well known systematic technique to find whether the mass transport is dominated by bulk diffusion or surface reaction is to compute the Biot number (Incropera et al., 2007), which for a spherical particle is:

$$\mathrm{Bi} = \frac{h_m r_0}{3\hat{\mathcal{D}}}, \tag{55}$$

where $\hat{\mathcal{D}}$ is an effective bulk diffusion coefficient (cm^2/s) and h_m is the surface mass transfer coefficient (cm/s). The use of such a mass transfer coefficient assumes that the transport processes are linearly proportional to species concentrations. Our model is quite nonlinear, but for this purpose, we can still construct this approximation. The surface mass transfer coefficients are derived from (6) and (7) by setting (Brenner and Leal, 1978):

$$\begin{aligned} s_{\mathrm{H}_b} &= h_{m,\mathrm{H}}(\mathrm{H}_b - \mathrm{H}_{b,s}), \\ s_{\mathrm{D}_b} &= h_{m,\mathrm{D}}(\mathrm{D}_b - \mathrm{D}_{b,s}), \end{aligned} \tag{56}$$

where $\mathrm{H}_{b,s}$ and $\mathrm{D}_{b,s}$ are the H and D saturated concentrations at the surface. They can be obtained from the equilibrium equations as:

$$\begin{aligned} \mathrm{H}_{b,s} &= \mathrm{V}_b \sqrt{[\mathrm{H}_2] K_{\mathrm{abs,H}}}, \\ \mathrm{D}_{b,s} &= \mathrm{V}_b \sqrt{[\mathrm{D}_2] K_{\mathrm{abs,D}}}. \end{aligned} \tag{57}$$

In this study, the Biot number from the simulation at $x_\mathrm{H} = 0.5$ is defined as the quadratic average over the H and D species:

$$\mathrm{Bi} = \frac{r_0}{3}\sqrt{\frac{h_{m,\mathrm{H}}^2}{\hat{\mathcal{D}}_{\mathrm{HH}}^2 + \hat{\mathcal{D}}_{\mathrm{HD}}^2} + \frac{h_{m,\mathrm{D}}^2}{\hat{\mathcal{D}}_{\mathrm{DD}}^2 + \hat{\mathcal{D}}_{\mathrm{DH}}^2}}. \tag{58}$$

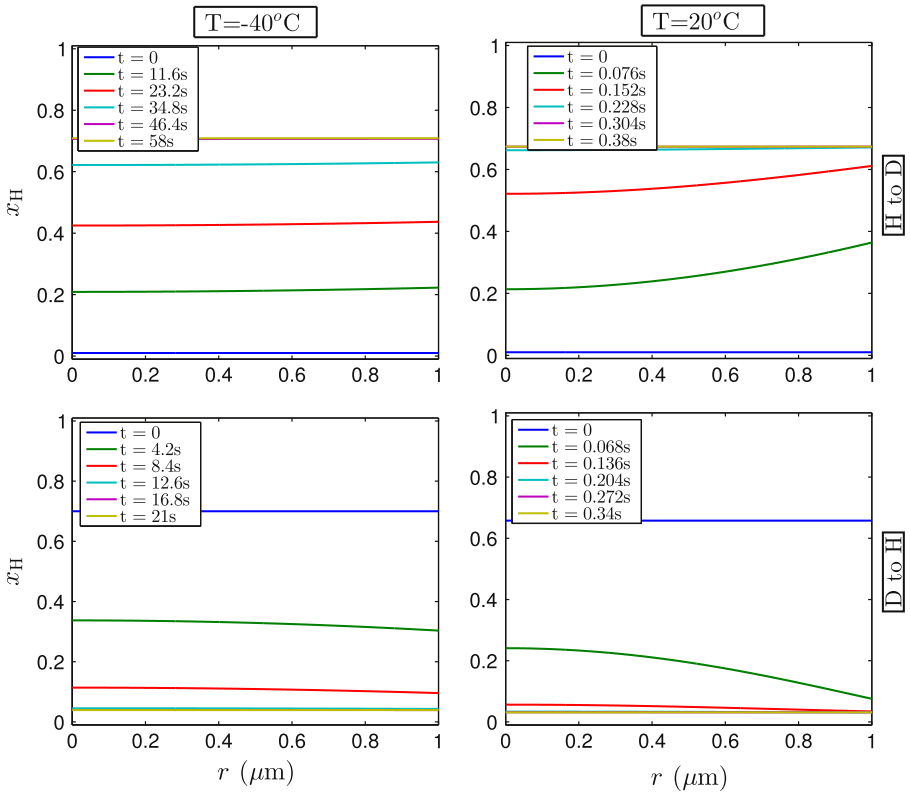

Fig. 4. Plots of the concentrations of the H species inside the hydride particle during isotope exchange at different times for the: (top row) "H to D" and (bottom row) "D to H" exchanges. The results are generated using the coupled surface reaction-particle diffusion model with a spherical particle of radius $r_0 = 1$ μm with a local pressure $P = 100$ kPa for $E_{ads,H} = -22.59$ kJ · (mol H)$^{-1}$ and two different temperatures, as indicated.

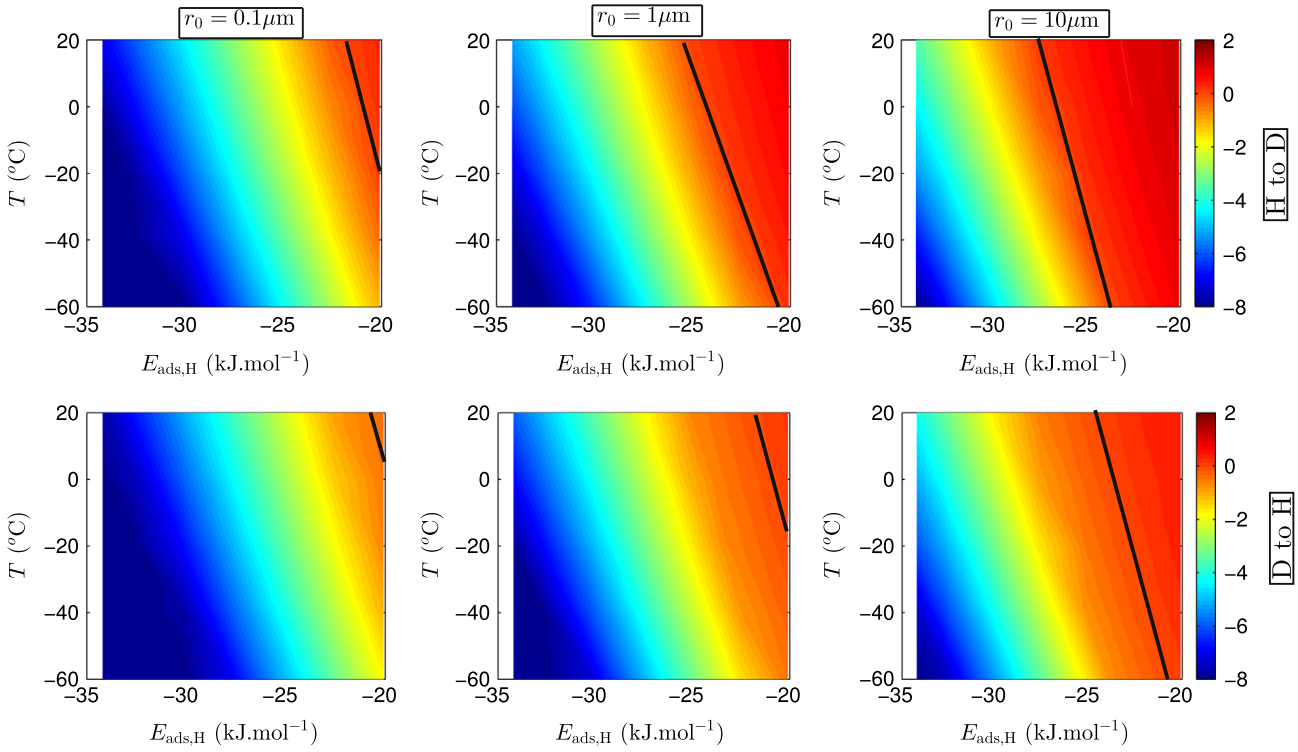

Fig. 5. Log base-10 Bi for the (top) "H to D" and (bottom) "D to H" exchanges as a function of the temperature T and the hydrogen adsorption energy, $E_{ads,H}$. Results were generated using the coupled surface reaction-particle diffusion model with a local pressure $P = 100$ kPa for different values of the particle radius r_0, as indicated. The solid black line distinguishes regions in which the exchange is limited by surface reaction toward the cooler colors or bulk diffusion toward the warmer colors.

where the $\hat{\mathcal{D}}_i$ are defined in Section 3.1. When $\mathrm{Bi} \ll 1$, diffusion is fast in the solid particle (Incropera et al., 2007) denoting a surface-limited exchange. Fig. 5 shows plots of the Biot number as a function of T and $E_{\mathrm{ads,H}}$ for different particle radii. The solid black line ($\mathrm{Bi} = 1$) delineates a boundary between regions in which the exchange is limited by surface reaction toward the cooler colors or bulk diffusion toward the warmer colors. Smaller particles, lower temperatures and higher adsorption energy magnitudes favor a surface-limited exchange. The "D to H" case favors the surface limited exchange, which is slower than in the "H to D" case because of the higher adsorption energy for D than H, so the areas of the warmer colored regions are slightly decreased.

6.2. Coupled surface reaction-gas flow model

As hydrogen gas is supplied to a PdD bed and when the surface kinetics are fast enough to be near equilibrium, a reaction front forms and moves along the bed such that the region upstream of the front is transformed into PdH. In the reverse reaction, deuterium is supplied to a PdH bed. In this case, exchange is enthalpically unfavorable, but it still occurs by equilibration of the solid with the deuterium-rich gas phase. A sharp reaction front does not form in this case. In both cases, the front is broader when kinetics are slow.

One concern when modeling reactive flow in a particle bed is that it is sometimes necessary to account for the species diffusion in the bulk solid particles. This would be the case when $\mathrm{Bi} > 1$ as discussed in Section 6.1. However, as mentioned in the introduction, the effects of the bulk diffusion are segregated from the reactive flow in the palladium powder bed by developing the two sub-models described in Sections 3.1 and 3.2. Hence, we assume the coupled surface reaction-gas flow model is operating in a regime where the bulk diffusion effects can be neglected (*e.g.*, small particle radii, see Fig. 5). Otherwise, an asymptotic analysis such as the linear driving force method (Glueckauf, 1955; Kim, 1989) must be invoked to account for diffusion in a computationally tractable manner.

Fig. 6 shows the normalized gas, surface, and bulk species concentrations along the bed during the reaction. The concentration profiles of hydrogen and deuterium follow similar trends in each phase: gas, surface, and bulk. Similarly to the coupled surface reaction-particle diffusion model, the "D to H" surface exchange is significantly slower than the "H to D" exchange demonstrated by the significant amount of D_2 gas breaks through the bed without reacting. In reactive flows, an important measure of reaction kinetics is the reaction front thickness, which in the present case can be taken as the width of the HD concentration profile (red curves in Figs. 6). In both "H to D" and "D to H" exchanges, the HD concentration distribution is narrower at 20 °C, representing a smaller reaction front thickness. This implies that the reaction is much faster at higher temperatures, as expected. There are about 40% vacancies in the hydride bulk, consistent with the amount found by the coupled surface reaction-particle diffusion model. On the other hand, the amount of surface vacancies is negligible, mainly because the surface states are very stable relative to the other phases, and the surface is mostly occupied by hydrogen or deuterium atoms.

Exchange kinetics can be studied by varying the values of both T and $E_{\mathrm{ads,H}}$, and plotting the associated HD concentration profile in the bed. Figs. 7 and 8 reveal that there is almost no exchange for $E_{\mathrm{ads,H}} = -35.14\ \mathrm{kJ\,(mol\ H)^{-1}}$ except at the highest temperature considered in the study (20 °C). Fig. 7 is the spatial mole fraction profile in the bed at a specific time, whereas Fig. 8 is the outlet concentration versus time. Gas closer to the outlet (higher values of z in Fig. 7) appears earlier in the time profile, so the figures appear to be mirror images of each other. Fig. 8 also reflects the time-dependent pressure profile, whereas Fig. 7 does not. The

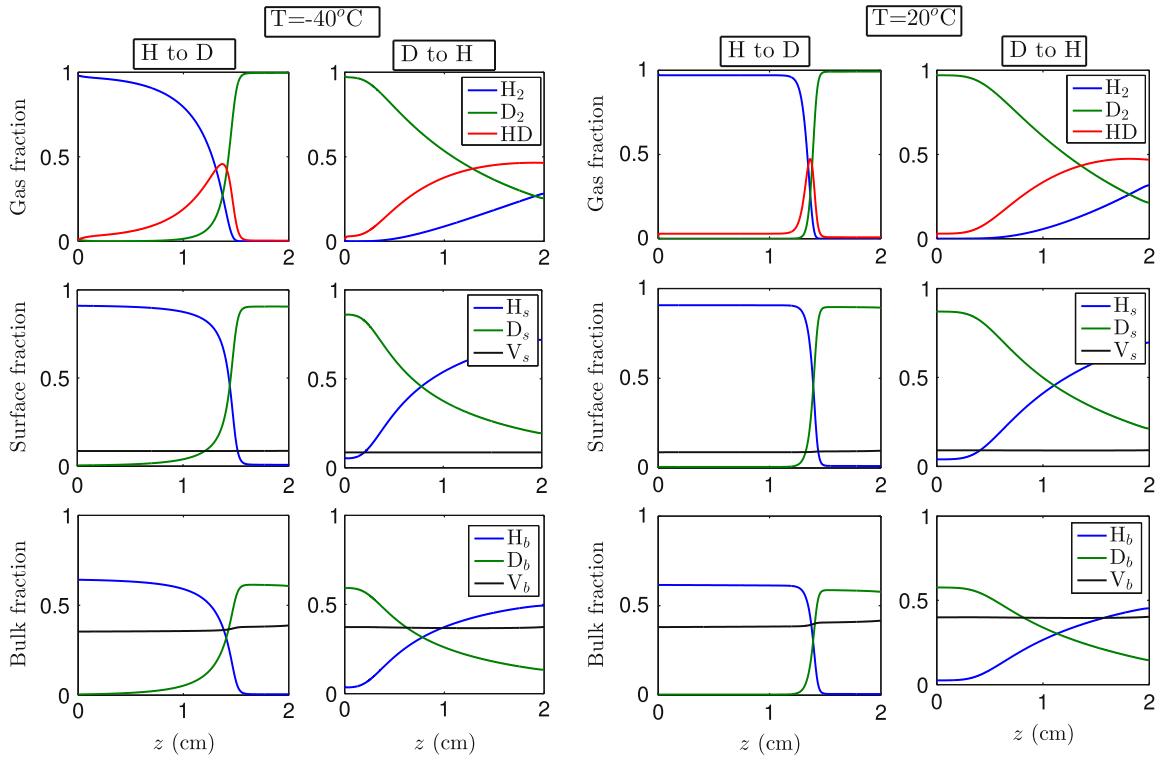

Fig. 6. Fractions of the (top row) gas species normalized by the total molar concentration, (middle row) particle surface species normalized by Γ_s, and (bottom row) particle bulk species normalized by Γ_b, as a function of the position within the bed z at t=20 s. Results are generated with $E_{\mathrm{ads,H}} = -22.59\ \mathrm{kJ \cdot (mol\ H)^{-1}}$ for both the "H to D" and "D to H" exchanges for T=-40 °C and T=20 °C.

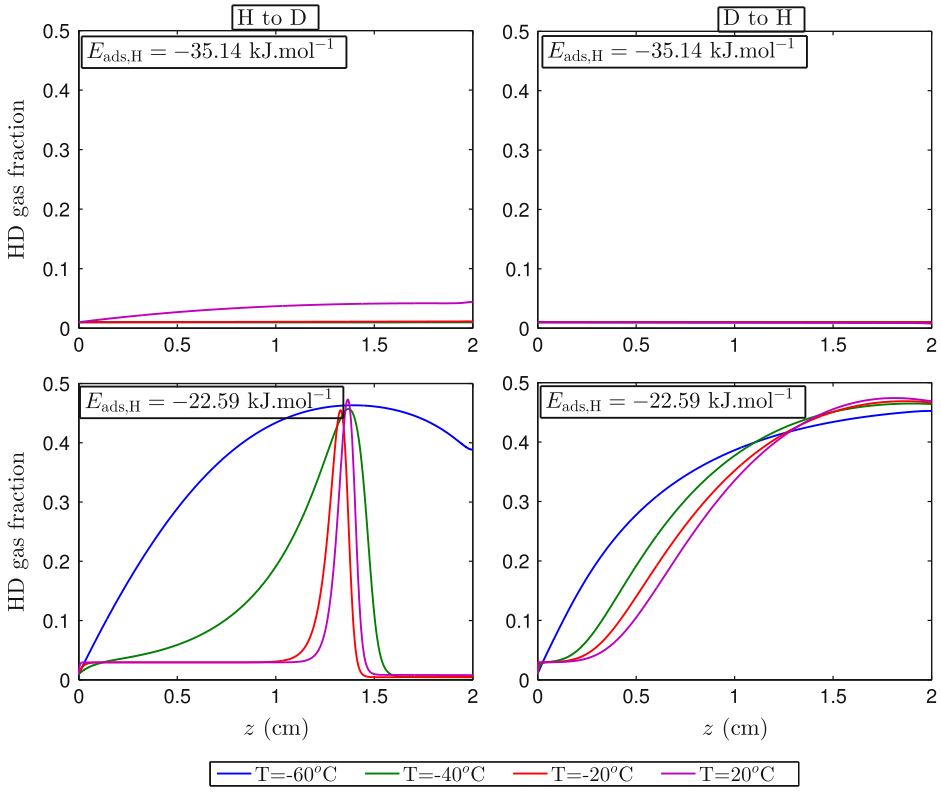

Fig. 7. Fraction of the HD gas normalized by the total molar concentration for (top row) $E_{ads,H} = -35.14$ kJ · (mol H)$^{-1}$ and (bottom row) $E_{ads,H} = -22.59$ kJ · (mol H)$^{-1}$, as a function of the position within the bed z at t=20 s. Results are generated for both the "H to D" and "D to H" exchanges and for different values of T as indicated.

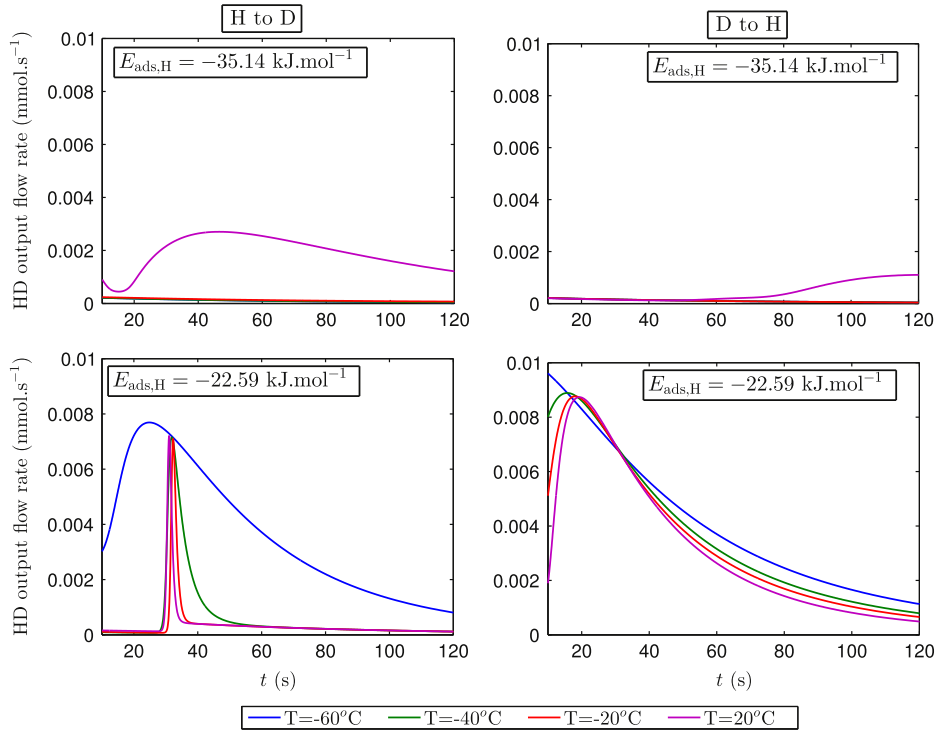

Fig. 8. Output flow rate of the HD gas as a function of time for (top row) $E_{ads,H} = -35.14$ kJ.(mol H)$^{-1}$ and (bottom row) $E_{ads,H} = -22.59$ kJ · (mol H)$^{-1}$. Results are generated for both the "H to D" and "D to H" exchanges and for different values of T as indicated.

asymmetry in the HD concentration profiles is mainly due to the non-uniform gas pressure and velocity considered in this study.

Next, the value of $E_{ads,H}$ is varied within a small range that was selected to obtain a fast exchange such that a reaction front is observed given the other parameters used in this simulation. The individual values of $E_{ads,H}$ were selected to understand the variability of the reaction rate as a function of temperature and exchange direction. The results are plotted in Figs. 9 and 10, which are related

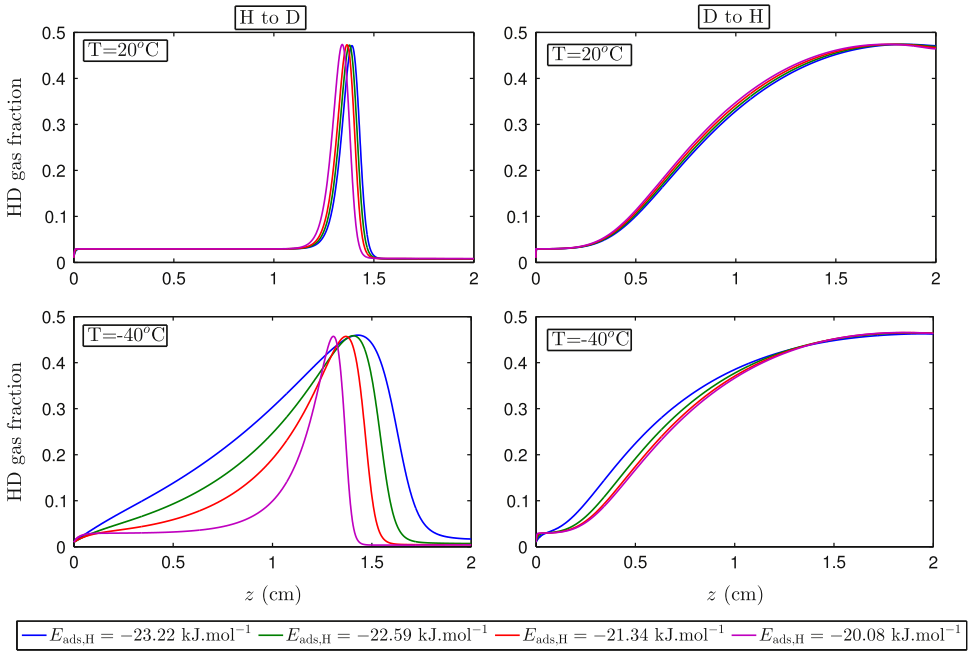

Fig. 9. Fractions of HD gas normalized by the total molar concentration for (top row) T=20 °C and (bottom row) T=-40 °C, as a function of the position within the bed z at t=20 s. Results are generated for both the "H to D" and "D to H" exchanges and for different values of $E_{ads,H}$ as indicated.

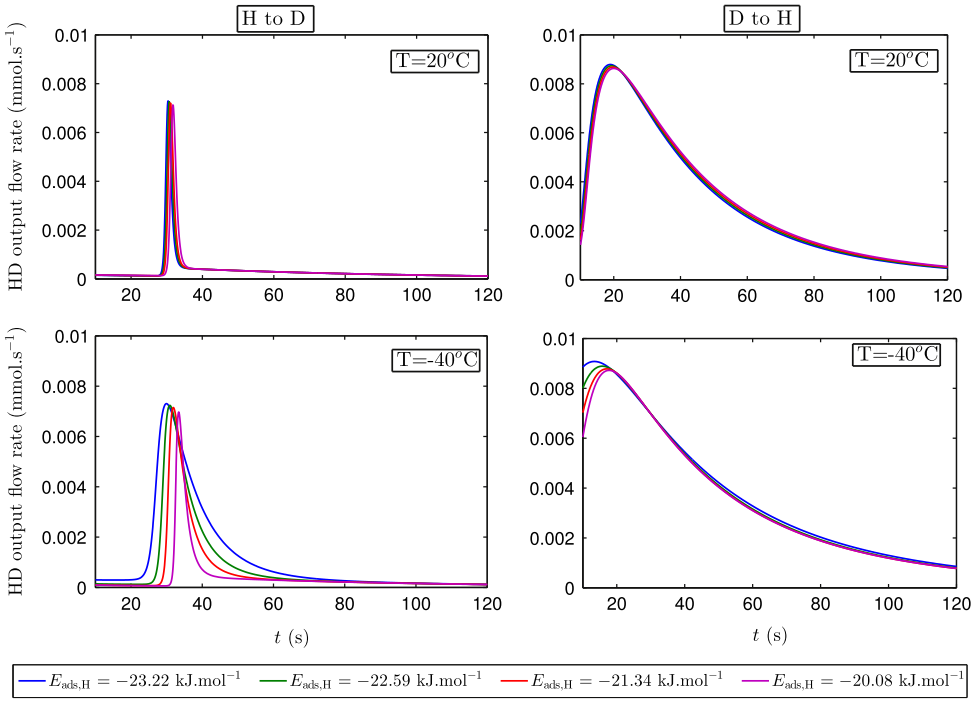

Fig. 10. Output flow rate of HD gas for (top) T=20 °C and (bottom row) T=-40 °C, as a function of time. Results are generated for both the "H to D" and "D to H" exchanges and for different values of $E_{ads,H}$, as indicated.

in the same way as Figs. 7 and 8. At T=20 °C, minimal variation in the reaction kinetics is observed. However, at T=-40 °C in the "H to D" exchange, there are substantial changes in the kinetics. This is not surprising given the non-linearities, especially those from $\exp(E_{ads}/RT)$ term. The overall effect is that at high temperatures, the exchange reaction is so fast that surface adsorption does not limit the process. Gas-phase axial diffusion is the other broadening mechanism built into the model, and this will lead to a lower bound on HD peak width when the chemical reaction is near equilibrium. The reaction does limit the process at low temperatures such that small variations in $E_{ads,H}$ induce significant variations in the overall performance of the reactor bed. For "D to H", the variation of $E_{ads,H}$ has a negligible effect on the concentration and flow profiles. Adsorption does not as strongly limit the surface reaction in this case, because the timescale of the "D to H" exchange is longer than that of "H to D" exchange, allowing the reaction to remain closer to equilibrium.

Two important design and analysis variables are the reaction front width and the number of theoretical plates, as recognized by Fukada et al. (1995). The latter is proportional to the square of the

ratio of bed length to reaction front width, and is a measure of the efficiency of the isotope exchange (Grob and Barry, 2004). In other words, more plates signify an easier and more complete exchange. The reaction width is defined here as the region in the bed where the HD gas fraction is larger than 0.01. As a separate measure, the number of plates can be defined as Grob and Barry (2004):

$$N_p = 5.54\left(\frac{t_{elution}}{t_w}\right)^2, \tag{59}$$

where t_w is the full width at half-maximum of the HD flow rate profile and $t_{elution}$ is the elution time when the reaction is complete and the reaction front peak exits the bed *i.e.*, when the HD flow rate is maximum (see Figs. 8 and 10). Note that we have defined the front width in terms of the spatial coordinate and the number of plates in terms of time.

The coupled surface reaction-gas flow model simulated different combinations of T and $E_{ads,H}$ and provided these two variables (front width and number of plates). An upper limit of 2 cm (bed length) for the front width was assumed for cases when both ends of the HD profile were not simultaneously present in the reactor.

Fig. 11 shows color plots of these two variables as a function of T and $E_{ads,H}$. The plots are not smooth due to the limited number of simulations performed using selected values of T and $E_{ads,H}$ (black dots); yet they reveal the trends in the reaction front width and in the number of plates. The reaction front width, w, decreases when the temperature increases and when the adsorption energy magnitude decreases, while the opposite takes place with N_p.

At low-magnitude values of $E_{ads,H}$, the variation of w and N_p is not monotonic as a function of temperature. At higher temperatures, diffusion gets faster, and the flow rate gets slower due to higher viscosity, allowing more time for axial diffusion. Also, while slower kinetics are expected at lower temperature, the stronger thermodynamic driving force for the "H to D" reaction is expected to contribute to a narrowing of the front width (Thomas, 1944; Luo et al., 2013).

The model can be used to optimize the pressure for a given set of conditions (*e.g.*, T and $E_{ads,H}$). Fig. 12 shows N_p as a function of inlet pressure at two different temperatures. An optimal inlet pressure exists that maximizes the number of plates in both cases. Gas chromatography theory predicts that an optimal flow rate exists that balances gas-phase diffusion, advection, and sorption-desorption kinetics (Clifford, 1989; Grob and Barry, 2004). The system described here differs from well established models of gas chromatography in various ways, including numerous nonlinear aspects to reaction kinetics and flow properties, and that the flow rate, which depends in the inlet pressure, changes over time and over the bed length. However, the overall concept of an optimal operating condition still applies. At pressures higher than the optimum, the experimental timescale gets shorter, and the kinetic limitation becomes increasingly important. At pressures below the optimum, the experimental timescale is longer. The chemical

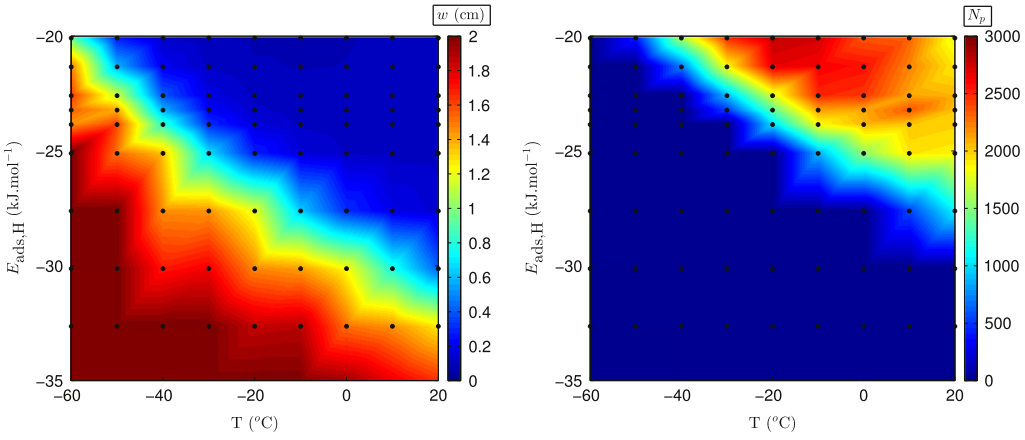

Fig. 11. (Left) reaction front thickness, w, and (right) the number of plates, N_p, as a function of temperature T and H_2 adsorption energy $E_{ads,H}$ for the "H to D" exchange. The black dots denote the values of the parameters $(T, E_{ads,H})$ where the computations were performed to generate the interpolated plot.

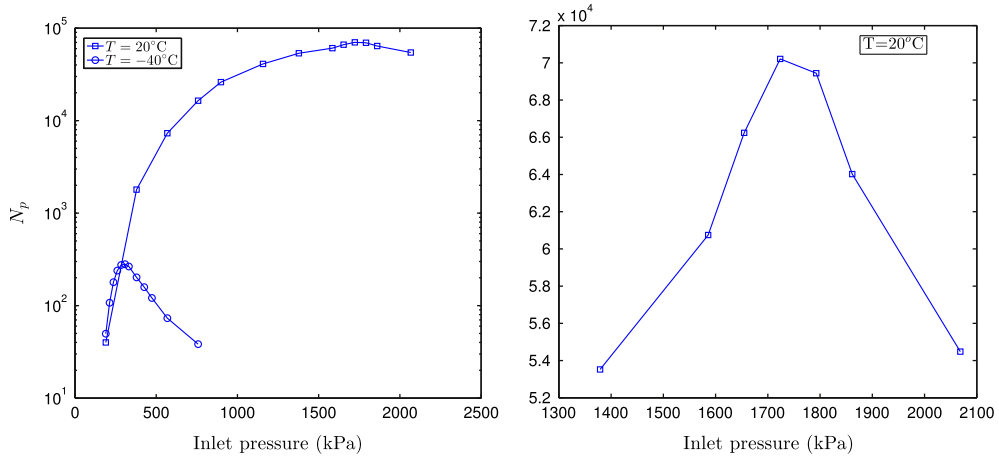

Fig. 12. Plots showing (left) the number of theoretical plates N_p as a function of the bed inlet pressure for two bed temperatures T=20 °C and T=-40 °C, and (right) a magnified view of N_p as a function of the inlet pressure for T=20 °C. The results were generated for the "H to D" exchange with $E_{ads,H} = -22.59$ kJ · (mol H)$^{-1}$.

reaction is closer to equilibrium, but diffusional broadening increasingly affects the result. At the optimal pressure range at −40 °C, the number of plates at 20 °C is comparable, but the number of plates at 20 °C continues to increase at higher pressures, whereas the kinetic limit sets in sooner at −40 °C.

Fukada et al. (1995) reported a comparable theoretical plate plot based on experimental data. They plot plate height, which is roughly equal to $0.2L/\sqrt{N_p}$. Eq. (27) and Table 5 can be used to show that the optimal velocity and optimal number of plates for their low temperature case is similar to that shown here. Their room-temperature values are not much higher, in contrast to our prediction. The activation energy that they report is comparable, so that is not the likely source of discrepancy. However, they do report complications associated with the cleaning of their sample, and arrive at a procedure that gives reproducible results, but may not have cleaned their surfaces to the point that our value of Γ_s is justifiable. Thus, it may be that Γ_s will prove to be as practically important as E_{ads} in comparisons with experiments.

7. Conclusion

The models described here are a useful set of tools for detailed investigations of the effect of surface reaction thermodynamics on hydrogen isotope exchange. For a given set of hypothetical reaction enthalpies, activation barriers, and attempt frequencies (each of which can be corroborated by separate experiments), and a given set of experimental conditions, the models can predict whether isotope exchange is limited by the surface reaction rate, or by other transport phenomena such as solid-phase diffusion within a hydride particle or axial diffusion in the gas phase.

The model captures our expectation that the stability of the surface hydride is a key parameter, inducing a large activation barrier to the surface reaction and a strong temperature dependence. A consequence of this is that there is a rather sharp transition between conditions where the isotope exchange reaction is limited by surface kinetics and those where the reaction is limited by solid-phase diffusion. This means that there are appreciably large regions of parameter space where one mechanism or the other can be neglected, and a simpler model used.

When solid-phase diffusion is much faster than the surface reaction, the flow model can be applied, and used to predict the pressure drop required to achieve the sharpest possible boundary between the isotopes, as measured by the number of theoretical plates. That optimum is predicted to be a strong function of the surface hydride stability and temperature. Comparison with the experimental results of Fukada et al. (1995) suggests that this function should not be so strong. Further experimental study of the chemical state of the surface may help identify the relative importance of blocked surface sites, as opposed to only the stability of available surface sites, and may help the efficacy of cleaning procedures.

The models presented here facilitate the design of experiments to gain a clearer understanding of the effects of surface thermodynamics (most notably surface activation energies) on the rates of interaction between palladium and hydrogen isotopes. For such a complex reaction environment, the models can help ensure that such experiments operate in a surface-limited regime, and the results are not influenced by convolution with other transport processes. Furthermore, the model will allow extraction of meaningful kinetic parameters from packed-bed isotope exchange experiments. This overall effort may result in palladium-based hydrogen separation and storage materials with surface composition and chemistry optimized for fast and efficient performance.

Acknowledgements

This work was supported by the Laboratory Directed Research and Development program at Sandia National Laboratories, a multiprogram laboratory managed and operated by Sandia Corporation, a wholly owned subsidiary of Lockheed Martin Corporation, for the U.S. Department of Energy's National Nuclear Security Administration under contract DE-AC04-94AL85000.

Appendix A. Supplementary data

Supplementary (list of symbols) data associated with this article can be found in the online version at http://dx.doi.org/10.1016/j.ces.2014.09.001.

References

Abbensetht, R., Wipf, H., 1980. Thermal expansion and lattice anharmonicity of Pd-H and Pd-D alloys. J. Phys. F: Metal Phys. 10 (3), 353–366.
Anthony, F. Mills., 2001. Mass Transfer. Prentice-Hall.
Bakaev, V.A., 2009. Inverse reaction chromatography. I: computer simulation of hydrogen/deuterium exchange on oxide surfaces. J. Phys. Chem. C 113, 13886–13893.
Bennett, P.A., Fuggle, J.C., 1982. Electronic structure and surface kinetics of palladium hydride studied with X-ray photoelectron spectroscopy and electron-energy-loss spectroscopy. Phys. Rev. B 26 (11), 6030–6039.
Brenner, H., Leal, L.G., 1978. Interfacial resistance to interphase mass transfer in quiescent two-phase systems. AIChE J. 24 (2), 246–254.
Charton, S., Corriou, J.P., Schweich, D., 1999. Modeling of hydrogen isotopes separation in a metal hydride bed. Chem. Eng. Sci. 54, 103–113.
Chen, Z., Huan, G., Ma, Y., 2006. Computational Methods for Multiphase Flows in Porous Media. SIAM Computer Science and Engineering, Philadelphia, PA.
Clifford, A.A., 1989. Theory of open-tube chromatography: an exact proof of Golay's equations. J. Chromatogr. 471, 61–69.
Conrad, H., Ertl, G., Latta, E.E., 1974. Adsorption of hydrogen on palladium single crystal surfaces. Surf. Sci. 41 (2), 435–446.
Dullien, F.A.L., 1979. Porous Media: Fluid Transport and Pore Structure. Academic Press.
Evans, L.C., 2010. Partial Differential Equations, Graduate Studies in Mathematics. American Mathematical Society.
Flanagan, T.B., Oates, W.A., 1991. The palladium-hydrogen system. Annu. Rev. Mater. Sci. 21 (12), 269–304.
Foltz, G.W., Melius, C.F., 1987. Studies of isotopic exchange between gaseous hydrogen and palladium hydride powder. J. Catal. 108, 409–425.
Fukada, S., Fuchinoue, K., Nishikawa, M., 1995. Isotope separation factor and isotopic exchange rate between hydrogen and deuterium of palladium. J. Nucl. Mater. 226 (3), 311–318.
Glueckauf, E., 1955. Theory of chromatography. Part 10: formulae for diffusion into spheres and their application to chromatography. Trans. Faraday Soc. 5 (1), 1540.
Greeley, J., Mavrikakis, M., 2005. Surface and subsurface hydrogen: adsorption properties on transition metals and near-surface alloys. J. Phys. Chem. B 109 (8), 3460–3471.
Grob, R.L., Barry, E.F., 2004. Modern Practice of Gas Chromatography, fourth ed. Wiley Interscience, Hoboken, NJ.
Heung, L.K., Sessions, H.T., Xiao, X., 2011. TCAP hydrogen isotope separation using palladium and inverse columns. Fusion Sci. Tech. 6, 1331–1334.
Incropera, F.P., DeWitt, D.P., Bergman, T.L., Lavine, A.L., 2007. Fundamentals of Heat and Mass Transfer. Wiley Interscience.
James, S.C., Hamilton, J., Wolfer, W.G., 2012. Diffusional exchange of isotopes in a metal hydride sphere. Chem. Eng. Sci. 68 (1), 250–257.
Jewell, L.L., Davis, B.H., 2006. Review of absorption and adsorption in the hydrogen-palladium system. Appl. Catal. A 310, 1–15.
Johansson, M., Sklason, E., Nielsen, G., Murphy, S., Nielsen, R.M., Chorkendorff, I., 2010. Hydrogen adsorption on palladium and palladium hydride at 1 bar. Surf. Sci. 604 (7-8), 718–729.
Kanouff, M.P., Gharagazloo, P.E., Salloum, M., Shugard, A.D., 2013. A multiphysics numerical model of oxidation and decomposition in a uranium hydride bed. Chem. Eng. Sci. 91, 212–225.
Kim, D.H., 1989. Linear driving force formulas for diffusion and reaction in porous catalysts. AIChE J. 35 (2), 343–346.
Larson, R.S., James, S.C., Nilson, R.H., 2011. Isotope exchange kinetics in metal hydrides I: TPLUG model. Technical report, Sandia National Laboratories, 2011. doi: http://dx.doi.org/10.2172/1030413.
Luo, W., Cowgill, D.F., Flanagan, T.B., 2013. Separation factors for hydrogen isotopes in palladium hydride. J. Phys. Chem. C 117 (27), 13861–13871.
Michalak, W.D., Miller, J.B., Alfonso, D.R., Gellman, A.J., 2012. Uptake, transport, and release of hydrogen from Pd100. Surf. Sci. 606 (3–4), 146–155.
Outka, D.A., Foltz, G.W., 1991. Mechanistic studies of the isotopic-exchange reaction between gaseous hydrogen and palladium hydride powder. J. Catal. 130 (1), 262–282.
Paglieri, S.N., Way, J.D., 2002. Innovations in palladium membrane research. Sep. Purif. Rev. 31 (1), 1–169.
Powell, G.L., Kirkpatrick, J.R., 1991. Surface conductance and the diffusion of H and D in Pd. Phys. Rev. B 43 (9), 6968–6976.

Rayhel, L.H., Corey, R.L., Shane, D.T., Cowgill, D.F., Conradi, M.S., 2011. Hydrogen NMR of palladium hydride: measuring the hydride-gas exchange rate. J. Phys. Chem. C 115 (11), 4966–4970.

Santandrea, R., Behrens, R., 1986. A review of thermodynamics and phase relationships in the palladium-hydrogen, palladium-deuterium and palladium-tritium. High Temp. Mater. Process. 7, 149–169.

Shugard, A.D., Robinson, D.B., 2014. A simple model of gas flow in a porous powder compact. Technical Report SAND2014-2858, Sandia National Laboratories, Albuquerque, NM, 2014. doi: http://dx.doi.org/10.2172/1127097.

Shugard, A.D., Buffleben, G.M., Johnson, T.A., Robinson, D.B., 2014. Isotope exchange between gaseous hydrogen and uranium hydride powder. J. Nucl. Mater. 447 (1–3), 304–313.

Thomas, H.C., 1944. Heterogeneous ion exchange in a flowing system. J. Am. Chem. Soc. 66 (10), 1664–1666.

Ward, T.L., Dao, T., 1999. Model of hydrogen permeation behavior in palladium membranes. J. Memb. Sci. 153 (2), 211–231.

White, F.M., 2006. Viscous Fluid Flow, third ed. McGraw-Hill, New York, NY.

Yun, S., Oyama, S.T., 2011. Correlations in palladium membranes for hydrogen separation: a review. J. Memb. Sci. 375 (1–2), 28–45.